PASSIVELY Q-SWITCHED ERBIUM-DOPED FIBER LASER USING SIDE-POLISHED FIBER AND 2D MATERIALS AS SATURABLE ABSORBERS

HAZIRAH BINTI HASSAN

INSTITUTE FOR ADVANCED STUDIES
UNIVERSITY OF MALAYA
KUALA LUMPUR

2019

PASSIVELY Q-SWITCHED ERBIUM-DOPED FIBER LASER USING SIDE-POLISHED FIBER AND 2D MATERIALS AS SATURABLE ABSORBERS

HAZIRAH BINTI HASSAN

DISSERTATION SUBMITTED IN FULFILMENT OF THE REQUIREMENTS FOR THE DEGREE OF MASTER OF PHILOSOPHY

INSTITUTE FOR ADVANCED STUDIES
UNIVERSITY OF MALAYA
KUALA LUMPUR

2019

UNIVERSITY OF MALAYA

ORIGINAL LITERARY WORK DECLARATION

Name of Candidate: **Hazirah bt Hassan**

Matric No: **HGG160001**

Name of Degree: **Master of Philosophy (Photonics)**

Title of Dissertation: **Passively Q-switched Erbium-doped Fiber Laser using Side-polished Fiber and 2D Materials as Saturable Absorbers**

Field of Study: **Photonics Engineering**

I do solemnly and sincerely declare that:

(1) I am the sole author/writer of this Work;
(2) This Work is original;
(3) Any use of any work in which copyright exists was done by way of fair dealing and for permitted purposes and any excerpt or extract from, or reference to or reproduction of any copyright work has been disclosed expressly and sufficiently and the title of the Work and its authorship have been acknowledged in this Work;
(4) I do not have any actual knowledge nor do I ought reasonably to know that the making of this work constitutes an infringement of any copyright work;
(5) I hereby assign all and every rights in the copyright to this Work to the University of Malaya ("UM"), who henceforth shall be owner of the copyright in this Work and that any reproduction or use in any form or by any means whatsoever is prohibited without the written consent of UM having been first had and obtained;
(6) I am fully aware that if in the course of making this Work I have infringed any copyright whether intentionally or otherwise, I may be subject to legal action or any other action as may be determined by UM.

Candidate's Signature Date:

Subscribed and solemnly declared before,

Witness's Signature Date:

Name:

Designation:

PASSIVELY Q-SWITCHED ERBIUM-DOPED FIBER LASER USING SIDE-POLISHED FIBER AND 2D MATERIALS AS SATURABLE ABSORBERS

ABSTRACT

Technology and applications of fiber optics have progressed rapidly in recent years. Fiber optics sensor has been commercialized successfully and well established in various industries ranging from biomedical to defense technologies. Passively Q-switching technique is suitable to obtain short and powerful pulse. For this technique, saturable absorber (SA) is an important device and has experienced rapid development from semiconductor-base to nano-sheet materials base. Eventhough passively Q-switched fiber lasers usually have very simple structures with SA placed inside the laser cavity, the repetition frequency depends on many other operations parameters. As for the side-polished fiber (SPF), the fiber side-cladding is removed to expose the core for the purpose of coating SA on its surface. This is to ensure the laser evanescent wave will interact with the SA due to the difference in refractive index between SA with its surrounding. SPF has a unique structure which the cladding is literally removed until reaching to the core so that the sensitivity of the SPF can be improved. This thesis also focuses on the Molybdenum disulfide (MoS_2) material which is one of the transition-metal dichalcogenides that is used as saturable absorber. MoS_2 has a unique characteristics because when it is in monolayer form, it becomes a direct bandgap of ~1.9 eV however when it is in multilayer forms, it will have indirect bandgap. In addition to that, Carbon Platinum (CPt) is also proposed as SA in this thesis. CPt is a new material that was used as SA to produce Q-switched fiber laser. CPt which in liquid form with volume of 25 μL is dropped onto the SPF using micro-pipette and it take 30 minutes to dry.

Keywords: side-polished fiber, saturable absorbers, passively-Q-switched.

LASER PASIF Q-SUIS GENTIAN ERBIUM-DOP MENGGUNAKAN GENTIAN GILAP SISI DAN MATERIAL 2D SEBAGAI PENYERAP TEPU

ABSTRAK

Teknologi dan penggunaan gentian optik telah berkembang maju sejak kebelakangan ini. Sensor gentian optik telah berjaya dikomersialkan dan berkembang dalam banyak bidang termasuk perubatan hinggalah pertahanan. Teknik Q-suis pasif sesuai digunakan untuk mendapatkan denyutan pendek dan berkuasa. Untuk teknik ini, penyerap boleh-tepu (SA) adalah alat yang penting dan telah berkembang pesat daripada semikonduktor kepada lembaran nano. Laser gentian pasif Q-suis mempunyai struktur yang sangat mudah tetapi kekerapan pengulangan bergantung kepada parameter lain dengan meletakkan SA ke dalam rongga laser. Bagi gentian gilap sebelah (SPF), lapisan luaran gentian optik digilap untuk mededahkan teras bagi tujuan salutan SA di permukaannya untuk mengesan spektrum laser yang disebabkan oleh perubahan indeks biasan kerana tindak balas SA dengan persekitarannya. SPF mempunyai struktur yang unik di mana lapisan luaran dikeluarkan sehingga mencapai teras supaya sensitivity sensor gentian boleh ditingkatkan. Thesis ini juga menumpu kepada molibdinum disulfida (MoS_2) yang merupakan salah satu daripada dichalcogenides peralihan logam yang digunakan sebagai penyerap boleh-tepu. MoS_2 mempunyai ciri-ciri unik kerana apabila ia dalam bentuk monolayer, ia memberikan jurang langsung ~ 1.9 eV namun bila ia berada dalam bentuk multilayer, ia akan menunjukkan nilai jurang tidak langsung. Di samping itu, Carbon platinum (CPt) juga akan digunakan dalam penyelidikan ini. Cecair CPt dengan isipadu sebanyak 25 μL dititiskan ke permukaan SPF menggunakan mikro pipet dan jangka masa untuk ianya kering ialah selama 30 minit.

Kata kunci: gentian gilap sebelah, penyerap boleh-tepu, Q-suis pasif.

ACKNOWLEDGEMENTS

In the name of Allah, the most gracious and the most merciful. Alhamdulillah, thanks to Allah for giving me strength to withstand all the challenges and successfully completed this work entitled "Passively Q-switched Erbium-doped Fiber Laser using Side-polished Fiber and 2D Materials as Saturable Absorbers".

First and foremost, I would like to express my appreciation and gratitude to my supervisor, Prof Harith bin Ahmad and Mr. Faizal for their great concern, persistent encouragement, valuable guidance, strong support and encouragements for every single enriching and thought provoking discussions which helped me to complete this research.

Lots of love and thanks to my family, especially my mother, Nafiah bt Ibrahim, who always gives strong support and encourage me to finish this research passionately. Also, I would like to thank my siblings as they always support me without fail.

Last but not least, I would like to thank my lab mates, Mahdi, Reza, Dr Amiri and Dr Zarif who always helped me whenever I need help. Not forgetting, my colleague at Photonic Reseach Centre (PRC), Fatimah, Aisyah, Syahirah, Adawiyah, Nabila, Farhana, Aina, Anir and Ezzaty for their endless support in order to complete my study.

A tree is known by its fruit, a man by his deeds. A good deed is never lost, he who sows a courtesy reaps friendship, and who plants kindness gather love.

TABLE OF CONTENTS

LIST OF FIGURES

LIST OF TABLES

LIST OF SYMBOLS AND ABBREVIATIONS

CO_2	:	Carbon dioxide
Er	:	Erbium
Yb	:	Ytterbium
Nd	:	Neodymium
Pr	:	Praseodymium
Tm	:	Thulium
Ho	:	Holmium
EDF	:	Erbium-doped fiber
ASE	:	Amplified spontaneous emission
EDFA	:	Erbium-doped fiber amplifier
TIR	:	Total internal reflection
SA	:	Saturable absorber
OTDR	:	Optical-time domain reflectometer
SESAM	:	Semiconductor saturable absorber mirror
NPR	:	Nonlinear polarization rotation
SWCNT	:	Single-walled Carbon nanotubes
NOLM	:	Nonlinear-optical loop mirror
1D	:	One dimensional
2D	:	Two dimensional
3D	:	Three dimensional
SPF	:	Side-polished fiber
GO	:	Graphene oxide
CNT	:	Carbon nanotube
TMD	:	Transition metal dichalcogenide

TI	:	Topological insulator
BP	:	Black Phosphorus
OSA	:	Optical spectrum analyser
SPR	:	Surface plasmon resonance
MoS_2	:	Molybdenum disulphide
CPt	:	Carbon Platinum
NA	:	Numerical aperture
RI	:	Refractive index
CW	:	Continuous wave
prf	:	Pulse repetition frequency
SMF	:	Single-mode fiber
TE	:	Transverse electric
TM	:	Transverse magnetic
QD	:	Quantum dot
DC	:	Direct current
TLS	:	Tunable light source
OPM	:	Optical power meter
LD	:	Laser diode
WDM	:	Wavelength-division multiplexing
PDL	:	Polarization dependent loss
H_2SO_4	:	Sulphuric acid
H_3PO_4	:	Phosphoric acid
$KMnO_4$	:	Potassium permanganate
H_2O_2	:	Hydrogen peroxide
HCl	:	Hydrogen chloride
OSC	:	Oscilloscope

FWHM	:	Full-width half-maximum
$MoSe_2$	:	Molybdenum diselenide
Ag	:	Silver
Bi_2Te_3	:	Bismuth telluride
RF	:	Radio frequency
SNR	:	Signal-to-noise ratio
FBG	:	Fiber Bragg-grating
YAG	:	Yttrium aluminium garnet
Cr^{4+}	:	Chromium ion
Co^{2+}	:	Cobalt ion
ZnSe	:	Zinc selenide
PbS	:	Lead (II) sulphide
V^{3+}	:	Vanadium
$MgAl_2O_4$	:	Magnesium aluminate

LIST OF APPENDICES

CHAPTER 1: INTRODUCTION

1.1 Optical Fiber

An optical fiber is an ideal waveguide, which has low power loss and flexible. Hence, in 1963, the first fiber lasers were invented by Elias Snitzer by employing optical fibers where the rare-earth elements were doped into the core as the gain medium. Currently, research shows that fiber laser presents numerous benefits compare to other types of lasers for example CO_2 laser, due to their high output power, high stability (all light enclosed into the core), smaller size and practically easy to use. Due to these intentions, fiber lasers become necessary in the area of laser study. Besides that, fiber lasers are broadly used in numerous functions for example telecommunication, medicine, spectroscopy and material processing (Sun, Hasan, et al., 2010). As for the gain medium, rare-earth elements were used as a dopant for single-mode fiber for instance erbium (Er^{3+}) and ytterbium (Yb^{3+}) in the core.

Furthermore, erbium-doped fiber (EDF) is commonly used as the gain medium that operates at 1550 nm wavelength. This fiber can be pumped with laser sources of different wavelength, which is 980 nm and 1480 nm (Mao, Jiang, Li, Chang, & Liu, 2009; Nishizawa, 2014). In order to fabricate the EDF, the core must be doped with Er^{3+} ions. The output spectral characteristic of the EDF is affected by the concentration ratio of the dopant ions.

An EDF laser consists of three energy levels which are E_1, E_2 and E_3. When 980 nm light was pumped, the electrons will be excited from ground-state energy, E_1 to the highest energy level, E_3. Basically, ions at E_3 are unstable and will fall down to the ground-state through two channels. Firstly, spontaneous emission takes place where the ions transition from E_3 to E_2 by non-radiative emission and decay to E_1. The photons are emitted in the 1520-1570 nm wavelength range. Light will be amplified during the spontaneous emission propagation through the fiber (Abedin et al., 2011), and this phenomenon is named as amplified spontaneous emission (ASE) which become the fundamental supply of noise for the arrangement. Secondly, the photons will undergo stimulated emission. This happens when spontaneous emission boosts to a suitable level of ion population inversion between E_2 and E_1 energy levels. At this moment, the freshly produced photons will be amplified through the fiber and thus the system will perform as erbium-doped fiber amplifier (EDFA) (Zhu, Qian, & Helmy, 2007).

1.2 Pulsed Fiber Laser

During the first decade of the twenty-first century, fiber lasers expanded from the testing room into abundant of applications all over the world (Glass et al., 2000; Slusher, 1999). Fiber lasers are not similar with conventional laser eventhough they are solid state laser to be exact. Due to the differences, in most cases fiber lasers constantly obtain greater electrical efficiency than conventional solid-state lasers with similar output power and their beams are of larger optical quality.

An optical fiber made up of thin strand of glass with diameter of several micrometers to over a milimeter, and meters long or can reach hundred of kilometers long in some cases (J. C. Knight, 2003; Russell, 2006). A basic fiber consists of several layers as depicted in Figure 1.1. The function of the core is to carry and guide the light and also consist of a cladding that have lower refractive index that enclose the core. Light is guided throughout the core by the phenomenon of total internal reflaction (TIR).

In this modern era, fiber-based laser become high interest in the scientific field due to the growing needs of the industry (Fermann & Hartl, 2013). Passively Q-switching method is very convenient to produde short and powerful pulse. By using this technique, saturable absorber (SA) is employed because it is crucial material and has undergoes speedy growth from semiconductor to nano-sheet materials (R. I. Woodward

& Kelleher, 2015). Q-switching method also can be applied in thousand applications for example optical time-domain reflectometer (OTDR), material processing and remote sensing (Delgado-Pinar, Zalvidea, Diez, Pérez-Millán, & Andres, 2006). Although passive Q-switched fiber lasers have very simple arrangement but the repetition rate rely on the many other operations parameters (Ren et al., 2015). In general, the Q-switched operation is achieved by placing the SA inside the laser cavity.

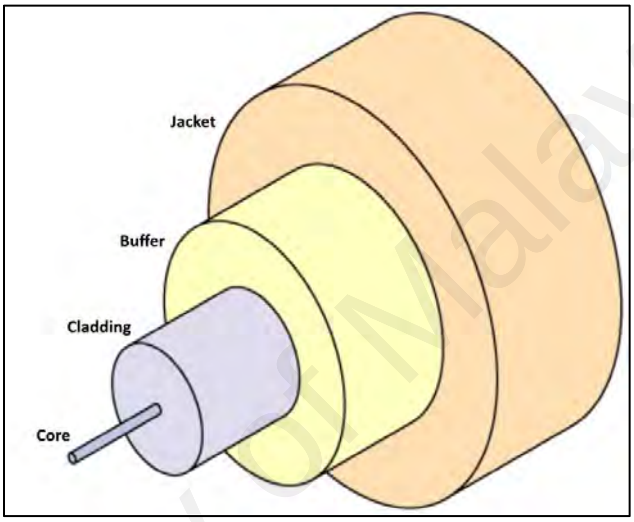

Figure 1.1: Basic structure of optical fiber

Previously, numerous techniques such as nonlinear polarization rotation (NPR), single-walled carbon nanotubes (SWCNTs), nonlinear-optical loop mirror (NOLM), semiconductor saturable absorbers (SESAMs) and graphene saturable absorbers (SA) have been used for generating stable Q-switching. Due to the ultrafast and zero band gap properties (Bao et al., 2009; Bonaccorso, Sun, Hasan, & Ferrari, 2010; Yamashita, 2012), graphene acts as an great SA and been braodly studied for the generation of ultrashort pulse in wide absorption spectral range (Popa et al., 2010; Sun, Hasan, et al., 2010; L. Zhao et al., 2010). The excellent achivements of graphene highly stimulate for further research of other graphene-like two dimensional (2D) materials for practical applications.

1.3 Side-polished Fiber

Side-polished fiber (SPF) is conventional optical fibers which one side of its cladding is partially removed to allow the evanescent field of light propagating through the fiber to radiate and interact with its surrounding (Ahmad, Amiri, et al., 2017). SPF has a unique structure where its cladding is literally removed until touching the core to improve the sensitivity of the fiber to the sorrounding (Lin Zhang, Zhang, & Bennion, 2008). The ability of producing the evenescent field in propagating beam has many advantages to the frequent tools used in optical system today for example directional couplers (Bergh, Kotler, & Shaw, 1980), polarizer (Eickhoff, 1980) and also modulators and switches (Markatos et al., 1987).

The working principle of the SPF core is depends on the interaction of powerful evanescent fields with surrounding media. They interact in close-spaced coupling between two metal layered on SPF fiber cores or by changing the medium layered refractive index on SPF. Besides that, the SPF also been examined as viable means to gain ultra-short pulses by non-linear saturable absorption method. This process is only available when the SPF has been coated with absorptive substances as depicted in Figure 1.2, such as graphene (Y.-W. Song, Jang, Han, & Bae, 2010) and graphene oxide (Jung, Koo, Debnath, Song, & Lee, 2012), carbon nanotubes (Liu, Chow, Yamashita, & Set, 2013; Y.-W. Song, Yamashita, Goh, & Set, 2007), topological insulators (Kowalczyk et al., 2016) and transition metal dichalcogenides (Sotor, Sobon, Grodecki, & Abramski, 2014; Wu, Zhang, Wang, Li, & Chen, 2015) and also unique substance for example black phosphorus (Park et al., 2015). The SPF exhibits characteristics that is very interesting due to its assymetric structure. Optical spectrum analyzer (OSA) able to scan the transmission and reflection spectra of output optical power.

Besides that, the effect of surface plasmon resonance (SPR) on SPF by using 2- and 3-dimensional materials can allow the interaction of free electrons in semitransparent noble metallic layer and light signal propagating inside the SPF. The excellent interaction between SPR and SPF can be applied in many sensing applications especially for biological and chemical components (Esmaeilzadeh, Arzi, Légaré, Rivard, & Hassani, 2015; J. Zhao et al., 2016).

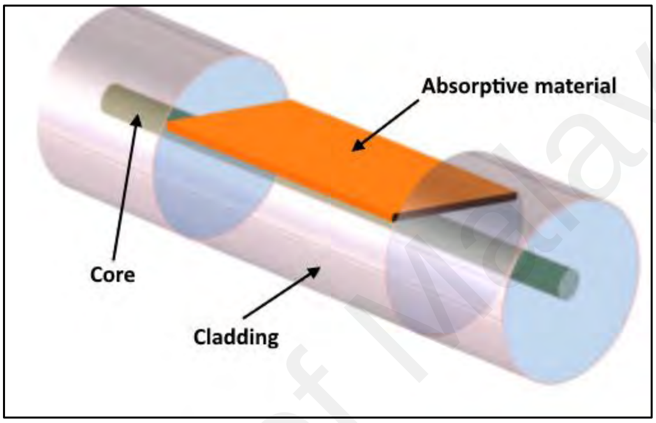

Figure 1.2: Schematic of the conventional fiber which its cladding partially removed

However, apart from its many possible applications, SPFs are normally not widely used in real-life because the price is slightly expensive due to complicated fabrication process. The fiber cladding elimination cause the fiber physically fragile and highly brittle (Kurkjian, Krause, & Matthewson, 1989; Senosiain, Díaz, Gastón, & Sevilla, 2001) and easy to break during the polishing process. In addresing this problem, researchers had carried out a lot of polishing methods such as etching the optical fiber that joined to a V-groove silica block (Tseng & Chen, 1992) and rotate a motor wheel to remove one side of the fiber surface (Hussey & Minelly, 1988; J. Zhao et al., 2015). Of all the designs, employing of polisher motor wheel could be most applicable because of its simple arrangement and it has many crucial advantages compare to other technique. Some of the benefits are short duration of polishing time and also made up of uncomplicated and low-cost fabrication arrangement. Most importantly, the success probability for this method is almost 100%, thus verify the fabrication devices based on the SPF significantly simpler and cost-effective.

1.4 Motivation

When comparing with the conventional optical fibers due to their small dimension and low loss, SPF exhibit many special characteristics include its powerful evanescent field interaction, clear surface field enhancement, able to generate ultra-short pulses and huge and uncommon waveguide dispersion. This special performances make them suitable for many applications in optical and photonics for example directional coupler, polarizers, modulator and sensing for biological and chemical (Esmaeilzadeh et al., 2015). Moreover, SPF also able to generate both Q-switched and mode-locked pulse fiber lasing with the aid of right saturable absorber materials (Kashiwagi & Yamashita, 2009; J Lee, Koo, Debnath, Song, & Lee, 2013; ZQ Luo et al., 2012). As for the conclusion, the motivation behind this work is to establish the SPF as the basis novel optical device that can be integrated into fiber laser particularly saturable absorber to obtain Q-switched operation.

1.5 Research Objectives

According to the motivation mentioned previously, the objectives of this research are as follows;

i. To implement new cost-effective and high efficient method to fabricate side-polished fiber.
ii. To characterize the side-polished fiber towards bending and temperature setting.
iii. To generate pulsed fiber laser using side polished fiber coated with 2D materials, which are Molybdenum disulphide (MoS_2) and Carbon platinum (CPt) as saturable absorbers for passive Q-switching.

1.6 Thesis Framework

This thesis consist of five chapters starting with Chapter 1 that briefly introduces the general background of the research study, motivation and objectives.

Chapter 2 explains the theory and literature review to provide an overview of the recent development in the field of fiber laser as well as the fundamental theory on evanescent field, propagation of light in SPF and as well as numerical aperture and acceptance angle. Further explaination about fiber laser and its type also discuss in this chapter.

Chapter 3 presents the research methodology including how to measure the non-linear absorption properties of Molybdenum disulfide (MoS_2) and Carbon platinum (CPt), fabrication of side-polished fiber and experimental setup for the generation of laser. The characteristics of side-polished fiber also been examined towards bending and temperature changes.

Chapter 4 reports and discuss about the performance of MoS_2 and CPt saturable absorbers in generating the Q-switching including their pulse width and repetition rate.

Last but not least, this research work reported in this dissertation is summarized in Chapter 5. An outlook on future research direction in this field is also suggested on the second section in this chapter.

CHAPTER 2: LITERATURE REVIEW

This chapter focuses on the theory and literature review related to optical fiber such as acceptance angle, numerical aperture and doped optical fiber which is used as the gain medium to generate laser. The chapter also enlightens the evanescent wave theory and what make it useful when interacting with surrounding. Besides that, this chapter also discusses about the methods of SPF's fabrication and the interaction of light propagating through it.

2.1 Acceptance Angle and Numerical Aperture (NA)

In order to verify that the light exactly confined inside the core, the upcoming light ray must be inside the core's acceptance angle, θ. The angle has been illustrated as an imaginary cone at the end of the fiber as illustrated in Figure 2.1.

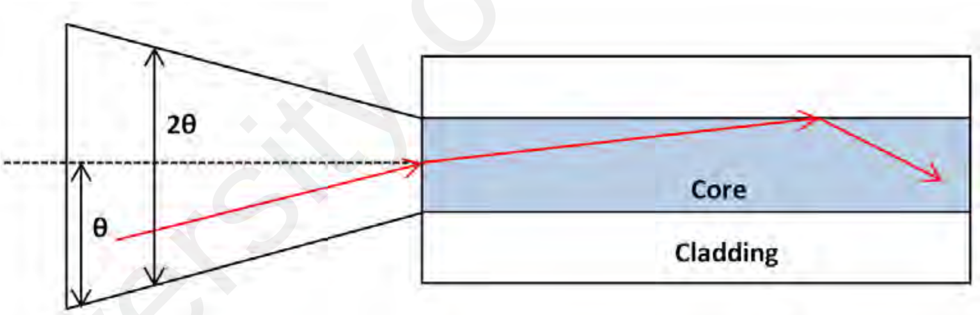

Figure 2.1: The rays that are enclosed within fiber core by total internal reflection

Furthermore, the NA is another important concept in fiber optic. It can be described as sine trigonometric of the core acceptance angle, θ as pictured in Figure 2.1. Snell's law proves that the NA is a function of refractive index (RI) of the fiber core and enclosing cladding as described in equation 2.1, whereby;

$$\text{Numerical aperture} = \text{NA} = \sqrt{n_{core^2} - n_{cladding^2}} \tag{2.1}$$

It is necessary to understand that the fiber physical aperture which is the core diameter has nothing to influence the NA. The NA only depends on refractive indices of the core and cladding (J. Knight, Birks, Russell, & Atkin, 1996; Leite et al., 2018).

2.2 Doped-optical Fiber

In fiber optic communications or beam delivery channel, the conventional optical fibers used are passive devices made up of pure glass cores which do not generate light. But, in optical communication system, the fiber lasers and fiber amplifiers are formed from fibers which the cores have been doped with impurities (Baker et al., 2017; Unger, Lindner, Aichele, & Schuster, 2018), as illustrated in Figure 2.2. Usually, the dopant used is neodymium, which the strongest laser line is at 1.06 µm (Ravi et al., 2017). However, ytterbium also widely used which have tunable wavelength lasing between 980 nm to 1.10 µm (Ahmad, Faruki, et al., 2017). Besides that, erbium is also used as dopant element with laser lines at 1.5 µm and 2.9 µm (Zheng, Ghandehari, & Ou, 2016). Last but not least, another dopant which is holmium has wavelength lines of 2.1 µm and 2.9 µm (Lancaster et al., 2015). Table 2.1 summarizes the selection of the impurities, which are the rare-earth elements with their emission wavelength.

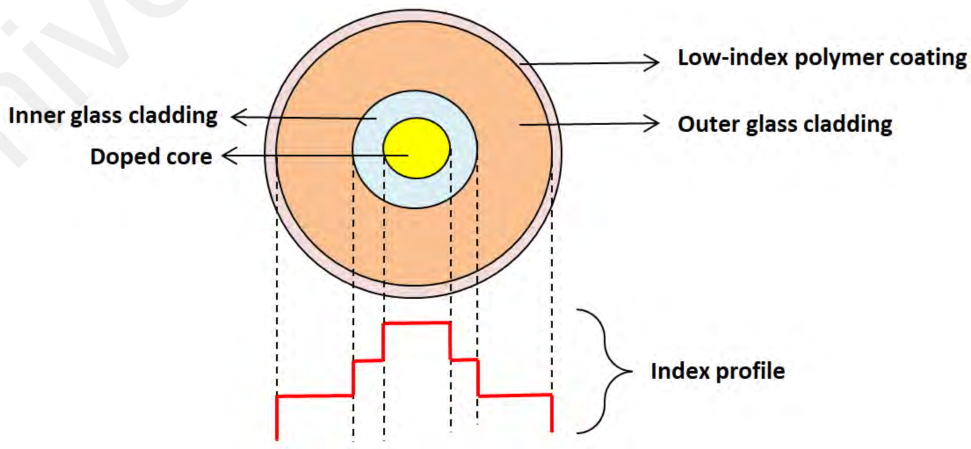

Figure 2.2: Doped-optical fiber and its index profile

In addition to that, fiber laser can be imagined as mirror-structures which both end will form a resonant cavity and cause the lasers to oscillate.

The difference between fiber lasers from standard solid-state lasers is their uncommon geometry which is very long and thin (Dong & Peng, 2015). Due to the unique geometry, the ratio of the surface area to the volume is much bigger than in a laser rod. This made them easier to expel waste heat and for sure excess heat is the limitation of solid-state laser.

Table 2.1: Rare-earth elements and their emission wavelength

Rare-earth Element	Emission wavelength
Erbium (Er)	1.1 - 2.9 µm
Ytterbium (Yb)	980 to 1100 nm
Neodymium (Nd)	1064, 1047, 1053, 1342, 946 nm
Praseodymium (Pr)	0.49, 0.52, 0.6, 1.3 µm
Thulium (Tm)	1.9 to 2.1 µm
Holmium (Ho)	2.1, 2.9 µm

Moreover, the long and thin configuration of fiber laser is responsible for generating higher power. With the tiny core, fiber laser can generate very high power densities which can avoid non-linear effects such as Brillouin scattering (Zervas & Codemard, 2014), stimulated Raman scattering (Gattass, Sanghera, & Shaw, 2017) and four-wave mixing (Boscolo & Finot, 2017) that change the laser light to different wavelength and cause the diminishing of the circulating power. The magnitude of these nonlinear effects is directly proportional with distance, which become highly effected in long fiber. Thus, the basic limitation on fiber laser is does not depends on heat elimination but the loss of intra cavity power due to nonlinear effects.

2.3 Q-switching

Q is stands for quality factor and Q-switching is one of the methods to produced pulsed output from a laser cavity. Pulsed lasers are beneficial in many applications instead of continuous-wave (CW) lasers which is not applicable in producing high power output (Keller, 2003). Energy from a pulsed laser is compacted into concentrated form. This concentrated energy in the laser pulse is stronger than the energy from CW laser.

The generation of Q-switched pulse can be described in few steps. Firstly, the losses of the cavity are kept at higher level. The energy sustain inside the gain medium by the pumping process accumulate as the lasing is not occur at this moment. The value of the stored energy is controlled by spontaneous emission or lasing as strong amplified spontaneous emission (ASE). The stored energy can be numerous of the saturation energy. Then, suddenly the losses decrease to a very low value and the laser radiation power boost rapidly in the laser resonator. This operation initiates with fluctuation of power from spontaneous emission and then magnified until macroscopic level within hundreds or thousands cavity round trip.

After that, when the intra cavity has achieved its saturation energy, the gain starts to saturate. At the moment when the gain equivalents to the remaining cavity losses, the peak of the pulse is achieved (Degnan, 1995; Keller, 2003; Spühler et al., 1999). The larger the intra cavity power at that moment, the further the depletion of the stored energy (Thurow, Satija, & Lynch, 2009). Normally, the energy obtained after the maximum pulse equals to the energy before the maximum pulse.

In addition to that, the pulse duration obtained with Q-switching is generally in nanosecond range. The generated pulse energy is normally greater than the gain medium saturation energy and can reach range of millijoule even for small laser. Besides that, the magnitude of peak power is greater than the continuous-wave generation.

Even the lasers having small size and focusing beam, the peak intensity enough for optical breakdown in air (Gattass & Mazur, 2008). When talking about the repetitive Q-switching, the pulse repetition rate is normally in the range of 1-100 kHz and sometimes can be higher. Passively Q-switched lasers have achieved the pulse duration greater than 1 nanosecond and repetition rate up to few MHz where basically laser configuration can give pulses with kilojoule of energy and duration of nanosecond range. Cavity losses can be achieved by two methods either active or passive.

2.3.1 Active Q-switching

In generating active Q-switching, the active element was adjusted to control the losses such as acousto-optic and electro-optic modulator (L. Liu et al., 2013). The pulse was built right after an electrical trigger signal appeared. Moreover, there is also mechanical Q-switch such as spinning mirror which is applied as end mirrors of laser resonator.

The repetition rate of the active Q-switching pulse laser can be adjusted by the modulator. Typically, higher repetition rate produced lower pulse energy if the pump power is not changed. The pulse also becomes longer as the initial gain become lower. In case of very high repetition rate, some pulses may be disappeared in the pulse train if the gain cannot recover the range of the time. Short energy pulses may be obtained for very low repetition rate but once the period is exceed the upper-state life-time, rising losses from spontaneous emission limit the possible pulse energy.

If the laser losses or laser gain are low, the generated pulse period is at least the resonator round-trip time or can be longer than that. For higher pulse repetition rate, it normally difficult to get a very short pulse. However, it can be solved by cavity dumping method. Instead of employing an ordinary output coupler mirror, ‘closed’ low-loss resonator in one of the effective method to generate pulse.

2.3.2 Passive Q-switching

Passive Q-switching is generated when the losses are generally modulated by saturable absorber (Xie et al., 2012). The pulse is obtained as the gain medium stored energy has achieved a sufficient tremendous level. Basically, the pulse energy and period are constant and the change of pump power only effect the repetition rate of pulse.

For 1-micron YAG laser, the commonly used SA material for passive Q-switching is Cr^{4+} (Schepler, Smith, Heine, & Huber, 1993). Whereas for 1.5-micron erbium laser, there are cobalt-doped crystals such as Co^{2+}: $MgAl_2O_4$ and Co^{2+}: ZnSe (Denker, Galagan, Sverchkov, & Prokhorov, 2013; Young & Setzler, 2007) and other glasses which doped with PbS quantum dots. In addition to that, for 1.3-micron region, V^{3+}: YAG crystal is the most suitable material used for SA. Semiconductor saturable absorber mirror can be used in different wavelengths.

The reconstruction period of SA is normally longer than pulse duration so that the unwanted energy losses can be prevented. Nevertheless, the absorber should be quick enough to avoid premature lasing as the gain retrieve. Generally, SA only absorbs a small fraction of energy from the produced pulses and absorber does not reduce the efficiency of lasing power (Biagi, Margheri, & Menichelli, 2001).

When comparing between active and passive Q-switching, passive technique is simpler and cost-effective because it do not use modulator and electronic device (Zhengqian Luo et al., 2010; Sun, Martinez, & Wang, 2016). Passively Q-switched is also very suitable for higher pulse repetition rate. However, the energies of the pulse normally lower. External influence of the pulse is also not relevant except with an optical pulse from other source and it may also be disadvantageous that the pulse energy and period are normally more or less independent of pump power which only affects the pulse repetition rate.

2.3.3 Output Measurement of Pulse Laser

Measuring the output of CW laser is not complicated and simply straightforward because the energy flows evenly and steadily, as drawn in Figure 2.3, which is different from pulsed laser. In measuring CW laser, the amount of output energy is measured against period of time.

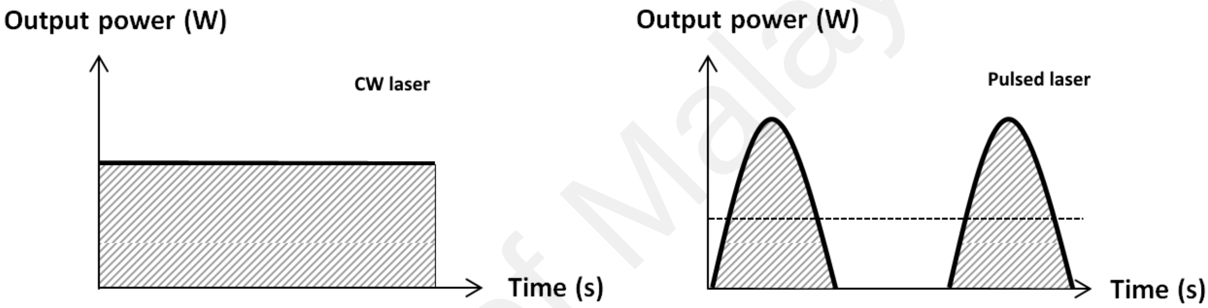

Figure 2.3: The shaded areas represent the energy produced in concentrated form by pulse laser. The peak power of pulsed laser is higher than CW laser

In addition, pulsed laser be measured by peak power and average power. The average power is the average rate of measurement at which energy flows from the laser for complete cycle.

Besides that, the pulse repetition frequency (prf) measures the emitted number of pulses that lase per second (Toth & Petrie, 2018). The pulse period is the time taken from the beginning of one pulse to another beginning of the next pulse which is in the form of reciprocal of the prf. The average power is the ratio of pulse energy and its period (Klenke et al., 2014):

$$P_{average} = \frac{Energy/Pulse}{Period} \quad (2.2)$$

Whereas, the peak power represents the ratio of the pulse energy to its duration (Kienel, Müller, Klenke, Limpert, & Tünnermann, 2016):

$$P_{peak} = \frac{Energy/Pulse}{Pulse\ Duration} \tag{2.3}$$

2.3.4 Quality of Laser Cavity

Q-switching is the simplest and commonly used concept in producing short pulse by controlling Q-factor or intra-cavity losses in the cavity. The storage of energy is in the form of population inversion so that it can achieve a certain level then will be delivered instantaneously in a huge pulse (Wong, Chen, & Sun, 2017). Normally, the pulse generation is in short duration of nanosecond to picosecond range. The quality of the laser cavity is represented in term of Q which carries information about the losses in the resonator. This Q-factor presents the laser resonator ability to maintain the energy (Basharin, Chuguevsky, Volsky, Kafesaki, & Economou, 2017). The higher the Q-factor, the lower the intra-cavity loss (Polak & Stothard, 2018). The Q-factor can be formularized as:

$$Q = \left(\frac{2\pi f_{\circ}\varepsilon}{P}\right) \tag{2.4}$$

where ε is the stored energy in the cavity, $f_{\circ}$ is the resonant frequency and $P = -\frac{dE}{dt}$ represent the power dissipated. The emitted laser is in the form of intense light than the continuous output laser. This technique is called Q-switching.

Nevertheless, the gain in the cavity will keep increasing as the energy is pumped into the cavity. The energy became saturated when it reached a maximum point. As a result, the energy is suddenly switching from higher energy level to a lower energy level (high loss energy) in the form of short and intense light. The pulse repetition rate typically in Hertz or a few Megahertz regimes which is lower than cavity round trip duration.

There are two techniques to produce Q-switched fiber laser, either by passive or active (C.-M. Chen, Lee, Huang, Chen, & Jiang, 2018; Wei et al., 2016). For active fiber laser, electro-optic and acousto-optic modulator is employed to adjust the cavity loss. By using the active modulation device, the losses of the cavity are changes according to external control signal. This active Q-switching has short pulse duration, more stable pulse repetition rate frequency, high power and smaller interpulse time jittering (Lü, Han, Liu, Chen, & Ren, 2014), hence produce more expensive and complex laser configuration.

2.4 Side-polished Optical Fiber

Sometimes this type of fiber also called as D-shaped fiber because of the formation of cross-sectional D-shaped structure as one side of the fiber has been polished. This fiber is produced either by mechanical polishing or chemical etching (X. Chen, Zhang, Liu, Hong, & Webb, 2015). Table 2.2 summarized the methods used to produce side-polished fiber and their performances. The production of strong evanescent field makes the propagation constant of the fiber become more responsive to the surrounding refractive index (Shivananju et al., 2017). Besides that, optical transmission attenuation is also caused by the interaction of evanescent wave on the surface of the fiber with surrounding environment. It is reported that when the light rays coupled out from the polished fiber into coated metallic nanostructures film, the active surface area can be increase by several level of magnitude.

Table 2.2: Methods used to produce side-polished fiber

Method	Insertion Loss (dB)	Polarization Dependent Loss (dB)	Refractive index	Reference
V-groove quartz block	1.7	1.36	-	(Junsu Lee, Koo, Jhon, & Lee, 2014)
Chemical etching (hydrofluoric acid)	-	-	1.33 - 1.37	(Coelho et al., 2015)
Aluminum oxide powder	-	-	1.49	(Bilro, Alberto, Sá, de Lemos Pinto, & Nogueira, 2011)

2.4.1 Interaction of Light Propagating in the Side-polished Fiber

In this research, the conventional SMF-28 is used in fabricating the SPF by creating 2 mm length of polished part. It is important to set in mind that the cladding thickness removal carries important role for SPF's efficiency to interact with the SA. Direct interaction of guided mode evanescent field and uneven fiber surface that surrounds them lead to significant loss for the configuration (Amiri, Ariannejad, & Ahmad, 2016; Soltanian et al., 2016). Thus the cladding needs to have greater than few micrometer of thickness (Yeom, Park, & Kim, 2004). Figure 2.4 shows the propagating field interaction between evanescent field and environment surrounding the cladding.

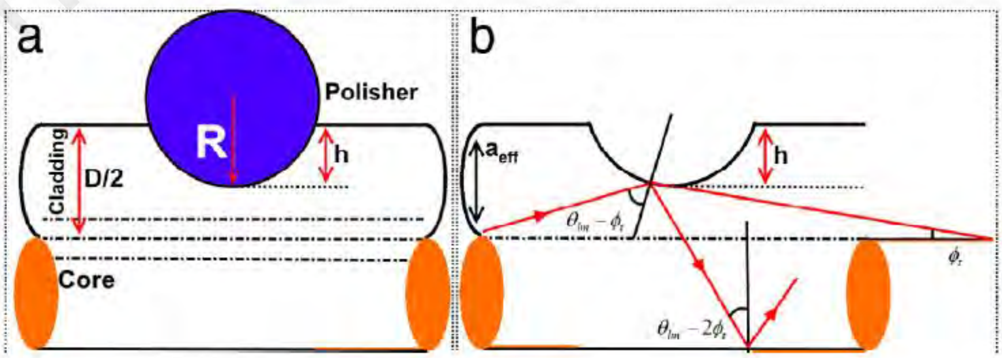

Figure 2.4: (a) Schematic diagram of SPF, where *D* is diameter of cladding, *h* is the penetration depth and *R* is the radius of the polisher. (b) Ray tracing within SPF, a_{eff} is the effective mode radius

The propagation mode can be changed to radiation mode via cut-off penetration depth (h_c). An incidence meridional angle , θ_{lm} and effective mode radius a_{eff}, complement each mode in radial order, m and azimuthal order (Cordaro, Rode, Barry, & Krchnavek, 1994; Kogelnik, 1988) can be defined as:

$$\theta_{lm} = \sin^{-1}(\beta_{lm} / kn_1) \tag{2.5}$$

$$a_{eff} = a + x_s(\theta_{lm}) \tag{2.6}$$

The propagation constant is describe by β_{lm} for the l_m mode while the increment created by the Goos–Hanchen shift is describe as x_s and $k = 2\pi/\lambda$ as the wave number. Assuming that $n_1 \approx n_2$, the TE and TM modes having the identical increment which can be determined from equation (Gloge, 1971) as follows:

$$x_s = 1/\left[k(n_1^2 \sin^2 \theta_{lm} - n_2^2)^{1/2}\right] \tag{2.7}$$

In the case if polished region diameter of optical fiber arrive a value of $r = a_{\text{eff}}$, the angle of reflection equals to $\theta_{lm} - \phi_t$, where ϕ_t is the angle between the tangential plane to the polished surface and the z-axis. It will then impinge on the diametrically opposite interface with an angle of incidence which is $\theta l_m - 2\phi_t$, in relation to the normal to the interface. So, the incidence angle will step toward the critical angle if only the thickness of the cladding is changed to its deepest point. The cut-off angle, $\O_c$ may be determined by the following equation:

$$\phi_c = (\theta_{lm} - \theta_{cr})/2 \tag{2.8}$$

where, the θ_{cr} is the total internal reflection. Thus, the cut-off penetration depth (h_c), can be work out as:

$$h_c = D/2 - a_{eff} + R(1 - \cos\phi_c) \quad (2.9)$$

The removal of cladding can be simply obtained by polishing and lapping method but need gentle care as the structure of fiber itself is very easy to over-polish and make the polishing reach the core if the process is not continuously supervised.

2.5 2D Saturable Absorbers for Fiber Laser

Nowadays, nanomaterials that have two-dimensional (2D) structure are rising and become latest materials for future photonics and optoelectronic operation (H. Zhang, 2015). There are many strategies for generating the emission of pulsed laser for example passive mode-locking (cavity-modes that have been phase-locked) or Q-switching (modulation of cavity Q-factor) by employing saturable absorber (SA) (R. I. Woodward & Kelleher, 2015). SA is a material which obeys an intensity-dependent transmission (W. Song et al., 2014) and frequently chosen as they provide wide-range of pulse parameters to be used without using expensive and complex electrically-driven modulators (R. I. Woodward & Kelleher, 2015) that ultimately impose a lower limit on the pulse durations achievable directly from laser source.

SA can be classified into two categories which are real and artificial SA. Real SA is the material that shows the reduction of intrinsic nonlinear absorption when having high light intensity (Jadidi et al., 2016) while artificial SA is the material that exploits nonlinear effect to play the action of real SA by inducing intensity-dependent transmission (Kuan, Kao, Wang, & Lin, 2018).

The excellent progress in saturable absorbers is relatively parallel with the development of the laser. The earlier pulse generation of SA-based was in 1964, that utilized both "reversibly bleachable" dye and coloured glass-filter to Q-switch a ruby laser were accounted for only four years after Maiman's outstanding of laser operation

(Maiman, 1960). Figure 2.5 shows the evolution of the notable SA advances. After these underlying exhibitions, reversibly bleachable (or saturably absorbing) dyes were generally connected to mode-lock lasers, where the gain medium was likewise a dye, prompting the primary development of continuous-wave (CW) mode-locking (Ippen, Shank, & Dienes, 1972).

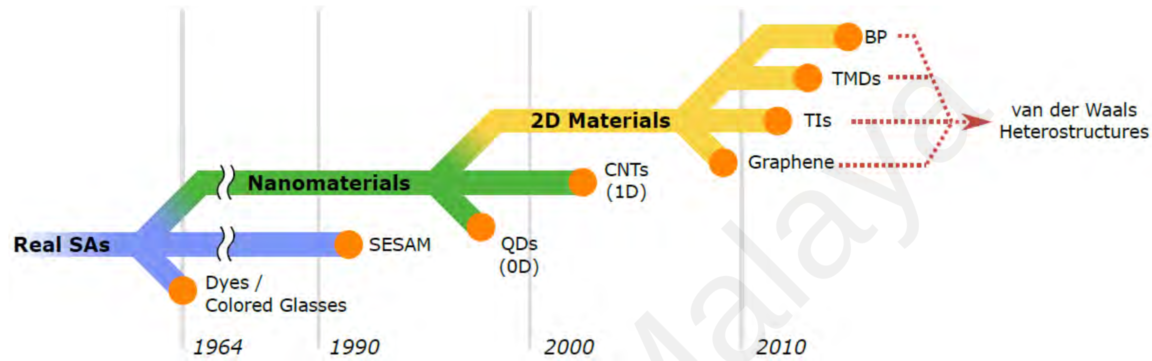

Figure 2.5: The development of real saturable absorbers

Source: (R. I. Woodward & Kelleher, 2015)

In early 1983, research continued with the development of the low-loss fiber optic which active doped fiber amplifiers for mode-locked laser until the report shown the unstable mode-locked of Nd fiber laser using a dye SA (Shi, Fang, Zhu, Norwood, & Peyghambarian, 2014). However, the used of SA in fiber system keep remained challenging for the generation of passive mode-locked until semiconductor saturable absorber mirror (SESAM) was introduced in 1990s.

Instantly, SESAMs became and remain to be outstanding technology in generate high energy Q-switched emission and ultrafast mode-locked pulses fiber lasers. But, SESAMs have limitation where it can operate in narrow bandwidth, need high cost for fabricating and the relaxation speed is limited to picosecond unless pricey post-processing method is used (Rahman et al., 2018). These limitations initiate the research into nanomaterials for SA application. The nanomaterials reduced the dimensionality which makes the SA into strong quantum confinement, new physical achievement and remarkable optoelectronics properties (Eda & Maier, 2013).

Early research of colored glass filter SA explored the nanomaterials since the glass used semiconductor nanocrystal as a dopant. The dopant is zero-dimensional quantum dots (QDs), such as cadmium selenide to change their colour (R. I. Woodward & Kelleher, 2015). Then in 1997 QDs were purposely used in the pulse generation. After that, the nanomaterials SAs gained traction as 1D carbon nanotubes (CNTs) and 2D graphene as materials that exhibit the intensity-dependent absorption and sub-picosecond relaxation time (R. I. Woodward & Kelleher, 2015).

Graphene is a single carbon atomic layer that obtained from graphite. Graphene exhibit 2D structure and zero bandgap which enable wideband optical operation (Novoselov et al., 2005). Yet, graphene is only one of the 2D materials that become monolayer and few-layer crystals from a variety of bulk materials including topological insulators (TIs), transition metal dichalcogenides (TMDs) and black phosphorous (BP) (Novoselov et al., 2005; Q. H. Wang, Kalantar-Zadeh, Kis, Coleman, & Strano, 2012; Xia, Wang, & Jia, 2014; Y. Zhang et al., 2010).

Of all these materials, they show specific yet complementary characteristic which bring new possibilities in optical applications fiber-based system. The combination of 2D materials to make heterostructure of van der Waals force also provide an special prospect for wide range of recent photonics device (Geim & Grigorieva, 2013) as the potential to make variety of nanomaterial characteristics for their growth conditions, doping and electronic control (E. J. Lee et al., 2015; Lin et al., 2015).

CHAPTER 3: EXPERIMENTAL METHOD

This chapter reveals the fabrication and characteristics of SPF including its stability towards bending and temperature with different insertion loss which are 1.50, 5.27 and 12.39 db. The fabrication of SPF is accomplished using conventional single-mode fiber (SMF-28) with core and cladding diameter are 8.2 and 125 μm respectively. Besides that, this chapter also shows the experimental set-up and non-linear absorption properties of the SAs.

3.1 Fabrication of Side-polished Fiber

The polisher arrangement is depicted in Figure 3.1. In this arrangement, it is important to make sure the SMF-28 that is used to make SPF is tightly suspended above the polishing wheel during the polishing process. Two Newport M-562-D stage optical alignments with Newport 561-FH fiber holders are used for this purpose. The SMF-28 is prepared by stripping a 3 cm long portion of the fiber coating and then suspending it over the polishing wheel with L_o = 5.2 cm and thus $L_o/2$ = 2.6 cm. The SMF-28 is adjusted so that the centre of the stripped portion is located at $L_o/2$ from the edge of the either fiber holders, and cleans with alcohol to remove the dirt and polymer debris.

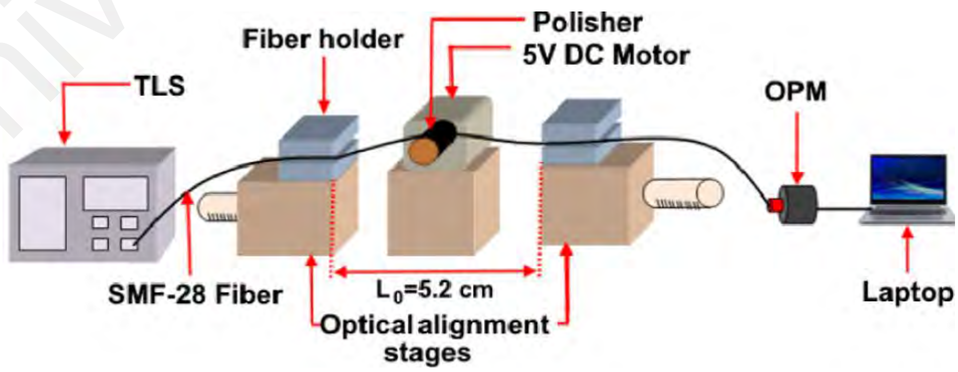

Figure 3.1: Polisher assembly set-up

The polishing wheel was made by wrapping scotch tape around 6 V DC motor shafts, followed by double sided tape (3M, 4011M- 10mm x 5 m/2131009). Then, silicon carbide paper with grit size of 400 is wrapped around the double sided tape to create a uniform polishing wheel having a diameter of 1.3 cm. The grit size is chosen over the other available grit size as a lower grit value will make the surface rougher and affect the SPF. This, a grit size of 400 gives a very smooth polish. The DC motor used has a maximum speed of 11442 rpm, with a torque of 1.4 x 10^{-3} Nm. The motor and wheel assembly as pictured in Figure 3.2 is then secured on a Newport M-561D alignment stage so that it lies perfectly perpendicular to and exactly in between the two translation stages.

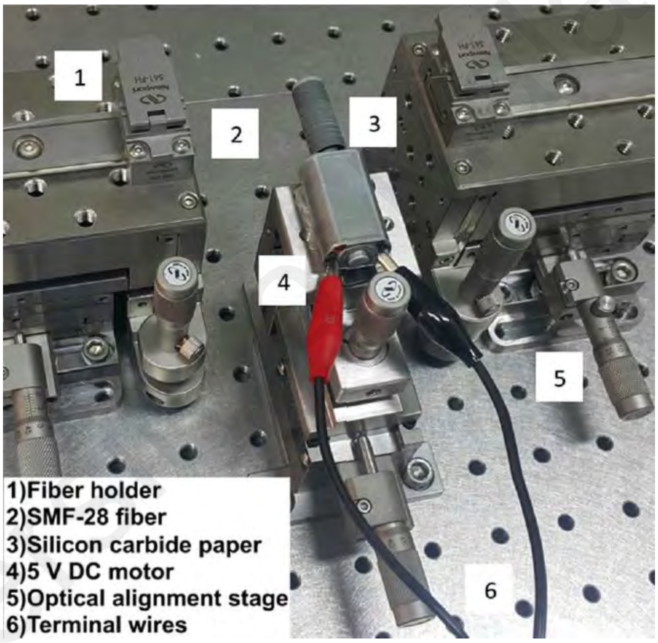

Figure 3.2: Image of actual side-polished fiber fabrication assembly

Firstly, before starting the polishing process, the rotating knob of the translation stage is adjusted so that the stripped part fiber attached to the wheel. A tunable light source (TLS) of 8 dBm power and 1550 nm is launched from one end of the fiber while the other end is connected with Thorlabs optical power meter (OPM) to monitor the power transmission along the polishing process. The rotation speed is set at 3.5 V. Not just monitoring the transmission power, the red light source or fault locator is also can be employed to observe the passage of light through to the stripped part of the fiber as shown in Figure 3.3. When the red light can be observe, the speed of the polishing motor is slow down to avoid from over-polished. The drop of power shows the polishing depth is approaching the core. Normally, the process takes at least 15 minutes to complete one SPF.

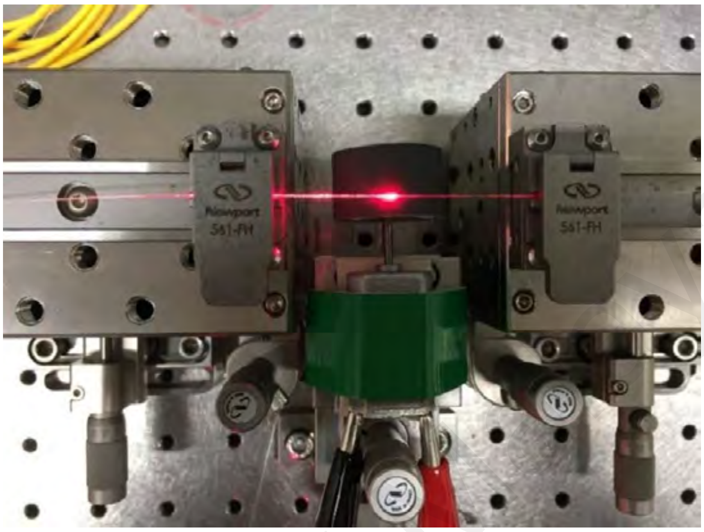

Figure 3.3: Visible red-light ‘leakage’ from polished part of SMF-28 indicates that the core has been exposed

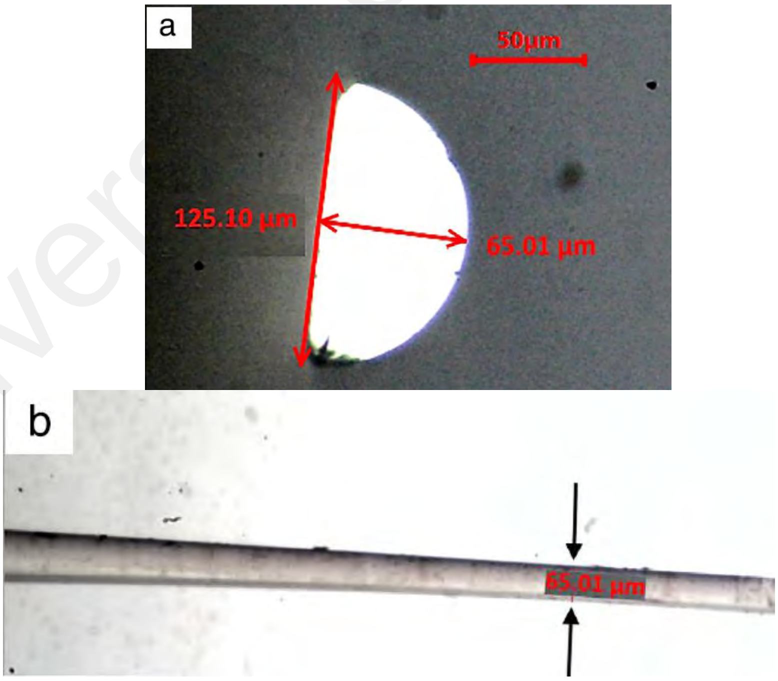

Figure 3.4: (**a**) cross-sectional view and (b) side view of the SPF

The original diameter of conventional SMF-28 is around 125.10 μm and after polishing process it reduces to only 65.01 μm with approximately 48% of the optical fiber has been removed, including about 2.0 μm of core. Figure 3.4 shows the cross-sectional and side views of the SMF-28 after the polishing process.

3.2 Experimental Set-up for Generating Fiber Laser

This section will cover up the details of experimental arrangement of the fiber laser and it is illustrated as Figure 3.5. This cavity made up of 3 meter length Fibercore M-12 Metrogain erbium doped fiber (EDF). The absorption coefficient of the EDF is 11.3 dB/m at wavelength of 979 nm. The mode field diameter and numerical aperture (NA) of the EDF are 6.6 μm and 0.21 respectively. The EDF undergoes backward pumped by a 1480 nm Fitel FOL140ZPLE-417 laser diode (LD). The LD pump the power through the 1480 nm port of 1480 / 1550 nm wavelength division multiplexing (WDM). The common port of the WDM is connected to the EDF while the other end of the EDF is connected to another similar WDM. The reason of using two WDMs is to remove any excess pump from the laser resonator and at the same time to optimize the performance of the laser system.

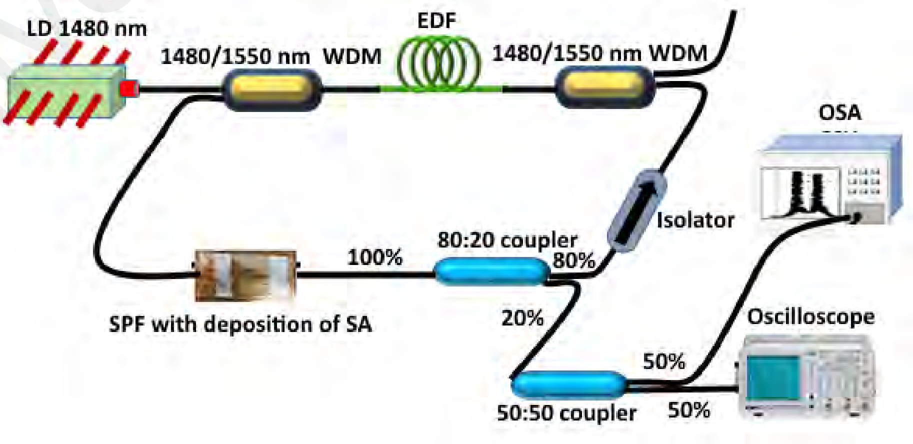

Figure 3.5: Cavity assemble for Q-switching pulse

As the EDF is pumped by the laser diode, amplified spontaneous emission (ASE) is developed. The ASE moves back towards the first WDM and directed to the 1550 nm port of the WDM which passes over the SPF that have been dropped with MoS_2 and CPt on its surface. The output laser travels throughout the cavity where it encounters 80:20 optical couplers. The signal analysis will receive 20% of the output while the 80% remaining will continue to circulate along the resonantor. The isolator is used to make sure the signal is passing in single direction only and finally completing the cavity by passing through 1550 nm port of the second WDM.

3.3 Characterization of Side-polished Fiber

The main characterization of this polished fiber can be divided into two, which are response against temperature and bending. The characterization process is also repeated by dropping Graphene oxide (GO) on the surface of SPF and again test the effect with temperature and bending.

3.3.1 Characterization of Side-polished Fiber against Bending and Temperature Noise

Fiber with different insertion losses were fabricated for this purpose. Various of different insertion losses of SPF are obtained from same polishing technique but different duration of polishing time by manipulating the voltage of DC motor. When reducing the DC voltage, the polishing time also will be delayed. Then, the desired insertion loss can be attained more precisely. When reaching the desire insertion loss, the polisher wheel is shifted away from the fiber. After that, gently apply alcohol on the fiber surface so that the measurement will be more accurate. Noted that, additional loss as high as 0.89 dB can be obtained if the fiber surface is not clean properly.

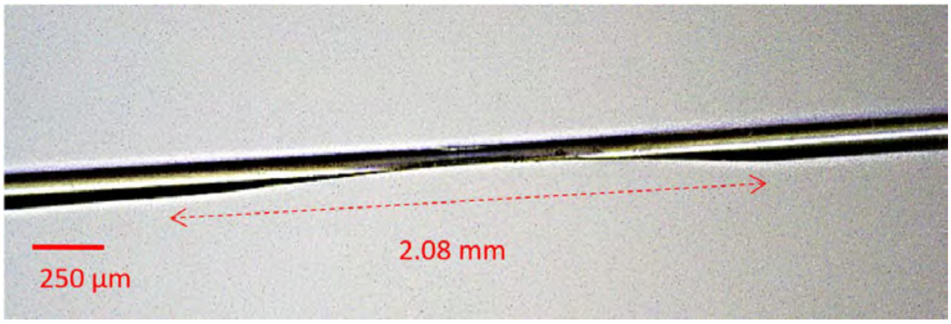

Figure 3.6: Image captured from microscope of SPF with 5.27 dB insertion loss

Figure 3.6 is a microscopic image of a fabricated SPF with an insertion loss of 5.27 dB and polarization dependent loss (PDL) of 0.59 dB. The arc-shaped side of the polished fiber also can be seen with its polished site to be approximately 2.08 mm long.

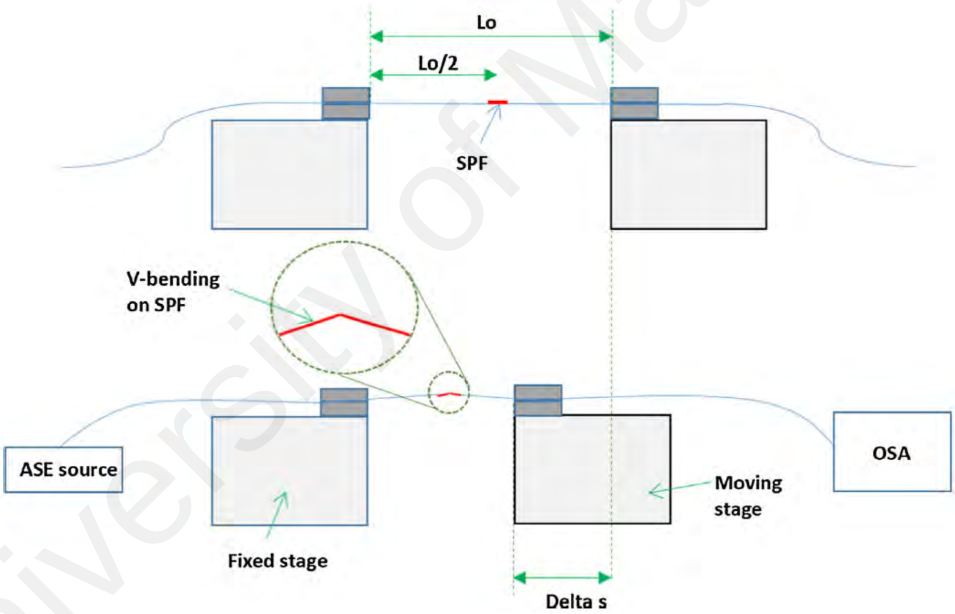

Figure 3.7: SPF bending experimental arrangement

The strength and durability of the fabricated SPF is examined by testing its bending and temperature changes. Figure 3.7 show the experimental arrangement applied to test the bending reaction of SPF. Two fiber holders were used to hold the SPF securely and tightly with L_o = 5.2 cm and the centre of SPF located at a distance of $L_o/2$ = 2.6 cm. The polished site is faced at the bottom part of the fiber for the purpose of this experiment.

To construct bending condition, the position of one translation stage will keep fixed where the other side will move horizontally. The initial state of the displacement is labelled as delta-s (Δs). The micrometer heads of the translation stage plays important role for the movement. C-band ASE source with an output power of about -7.5 dBm is passed into the SPF as a test signal. The output from the SPF is measured using an Anritsu MS9740A optical spectrum analyser (OSA) for different Δs values. All the spectral measurements are made at the resolution and span of 0.03 nm and 20 nm respectively.

Δs is widen from 0.0 to 200.0 μm at 100.0 μm steps then reduced back to its original state of 0.0 μm at 100 μm steps again. The measurement recorded shows that the SPF able to maintain its transmission power characteristic before and after the bending tests.

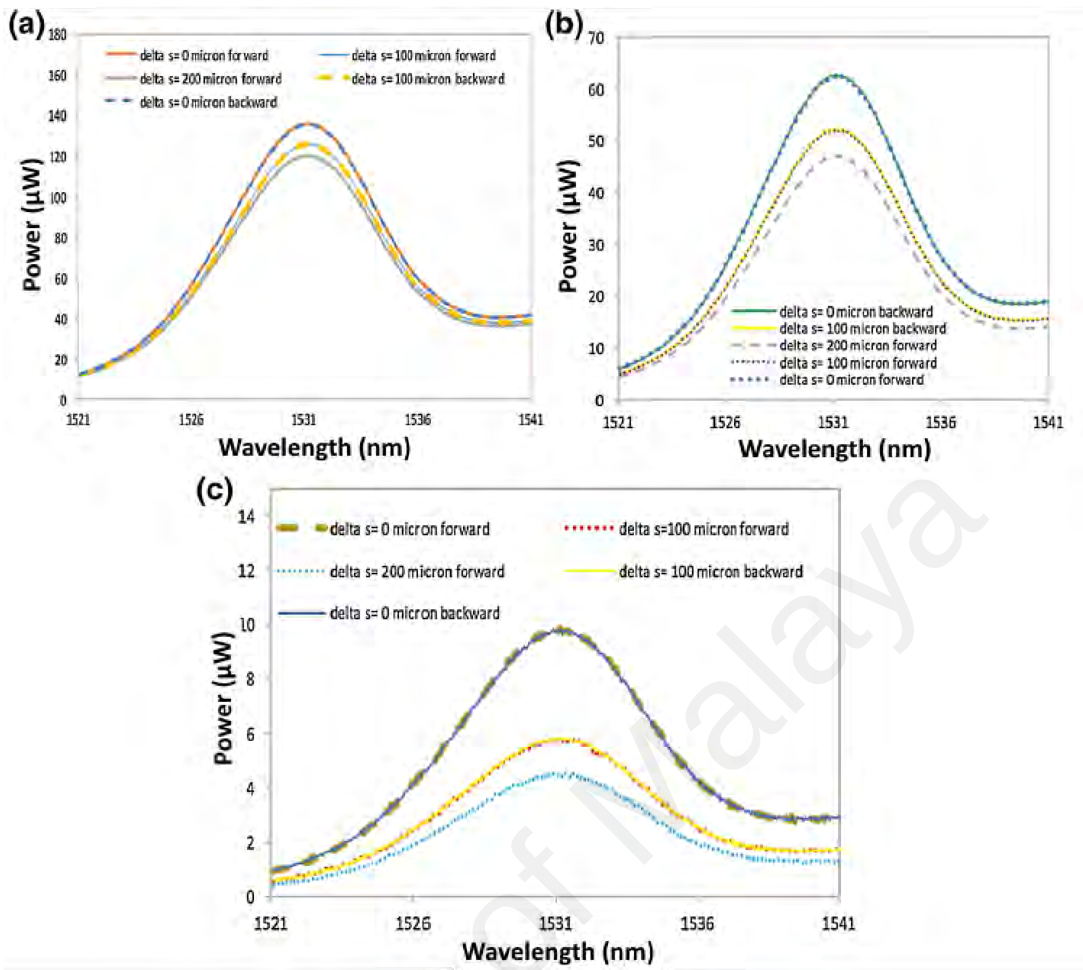

Figure 3.8: SPF ASE spectra for different bending condition of forward and backward translation with insertion loss of 1.50, 5.27 and 12.39 dB respectively

Figure 3.8 analyzed the achieved spectra for different insertion losses of SPFs which are 1.50, 5.27 and 12.39 respectively. The polarization dependent losses (PDLs) also give value of 0.23, 0.59 and 1.39 respectively. Refer to the plots, the designation of ''forward'' after the Δs values mean the Δs is increasing state while ''backward'' means the Δs is decreasing state. It can be seen that when the Δs increase, spectrum power is decreased. Moreover, no spectral deviations are observed when Δs returns to a value of 0.0 µm displacement, thus proving that the SPF maintains its transmission characteristics even after bending response.

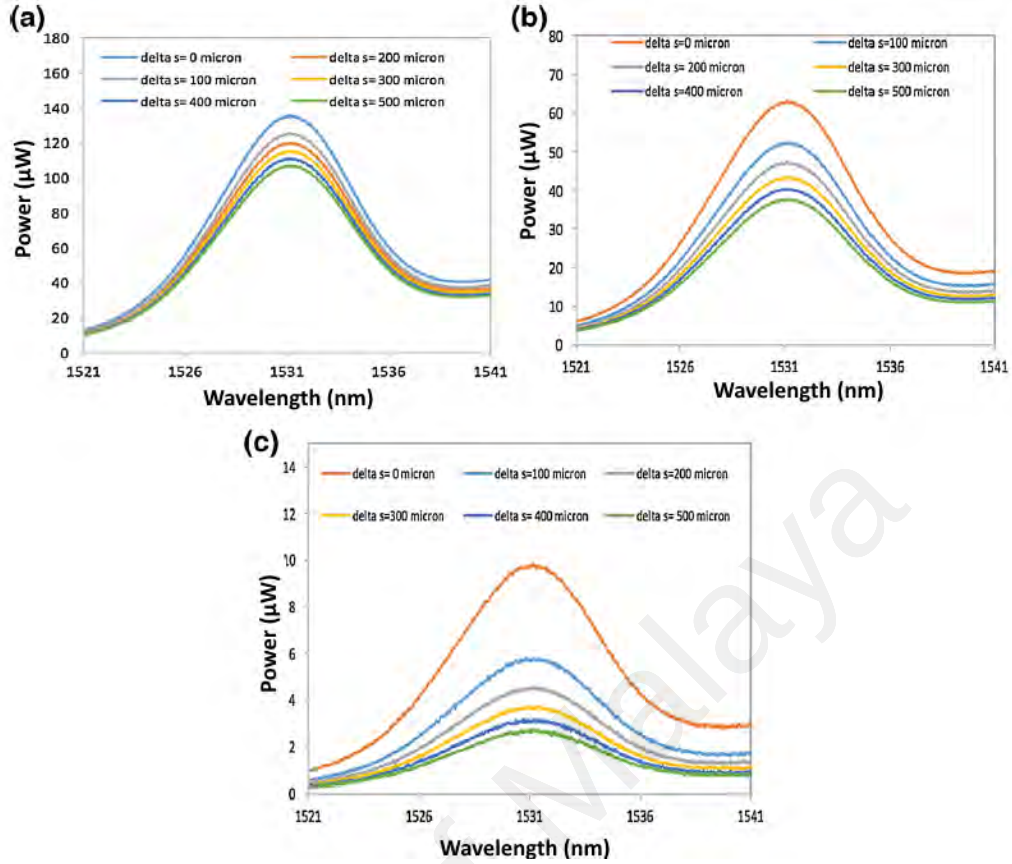

Figure 3.9: SPF ASE transmission spectra for different bending condition from Δs of 0 µm to 500 µm for 1.50, 5.27 and 12.39 of insertion loss respectively

Δs of the bending boundary are further extending until the values up to 500.0 µm with 100.0 µm step. Figure 3.9 draws the transmission spectral of three different insertion losses of SPFs with varies Δs value. The corresponding peak powers of ASE spectrum were plotted in Figure 3.10.

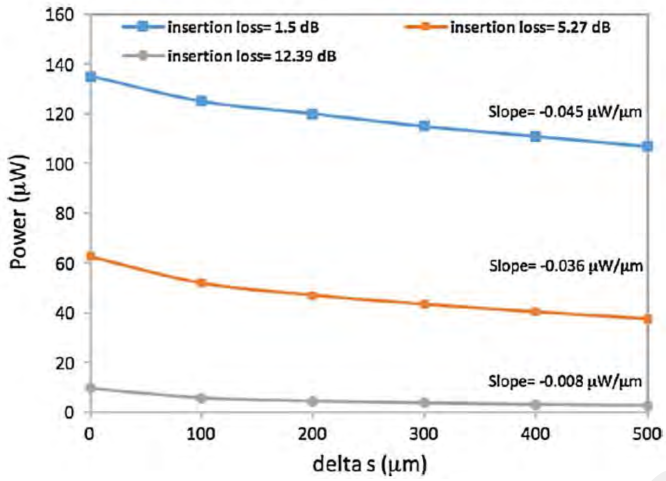

Figure 3.10: SPFs ASE spectra peak power at different insertion losses with different bending displacement

From the observation, the linearity is only obtained when Δs is above 100 μm. Higher spectral power change was presented when the fiber transition from straight manner to its initial bending condition compare to their subsequent bending displacement. Linearity slopes of -0.045, -0.036 and -0.008 dB/μm are achieved for the SPF insertion losses of 1.5, 5.27 and 12.39 dB respectively. Thus indicate the slope decreases as the insertion loss of the SPF increases.

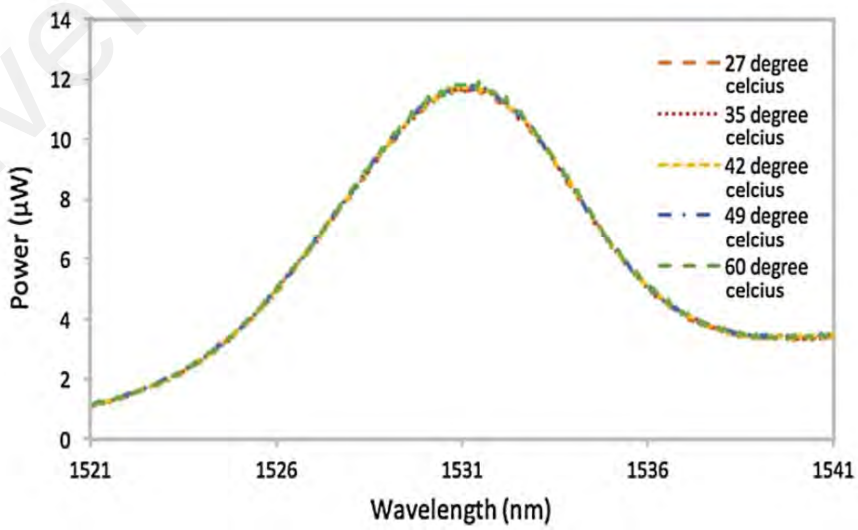

Figure 3.11: SPF ASE spectra at different temperature setting with insertion loss of 11.4 dB

This research also tested three SPFs with different insertion losses close to the previous towards the temperature response but the result of output power shows no significant change. Figure 3.11 plotted the transmission spectrum of SPF that having 11.4 dB insertion loss with different temperature change.

The test was run by sticking the SPF on a clean glass slide and put on a hotplate so that the heat is supplied from below of the glass slide. A thermocouple is employed to measure the temperature of the SPF while the ASE signal source and OSA settings are kept the same as before. The result achieved shows no significant spectrum change from 27 ºC up to 60 ºC which conclude that our fabricated SPFs is robust to temperature noise.

3.3.2 Characterization of Side-polished Fiber with Graphene Oxide Coating for Bending and Temperature Noise

This test was carried out similar as previous section but with addition of graphene oxide (GO) that has been dropped on the surface of SPF with 1.8 dB insertion loss. The GO was obtained from graphite flakes through chemical oxidation process. The procedure starts by pouring graphite flakes with 3 g weight into concentrated 360 ml sulphuric acid, H_2SO_4 and 40 ml phosphoric acid, H_3PO_4 while being stirring in an ice bath. Then, 18 g of potassium permanganate, $KMnO_4$ was poured to the mixture gently and the solution left for 72 h under stirring at room temperature. After that, 500 ml of distilled water was added and followed by 15 ml of hydrogen peroxide, H_2O_2 at 30% under ice bath so that the initial color dark brown turn to yellow. 250 ml of hydrogen aqueous solution, HCl 1M is used to wash the mixture. The washing process then proceeds by using deionized water to obtain the GO dispersion with acidity approaching pH 7. The method of GO deposition on SPF is drawn in Figure 3.12. Before dropping the GO, make sure the SPF has been cleaned with alcohol and it insertion loss also been noted. The polisher is bringing away from the vertical translation stage and replaced with hygienic glass slide.

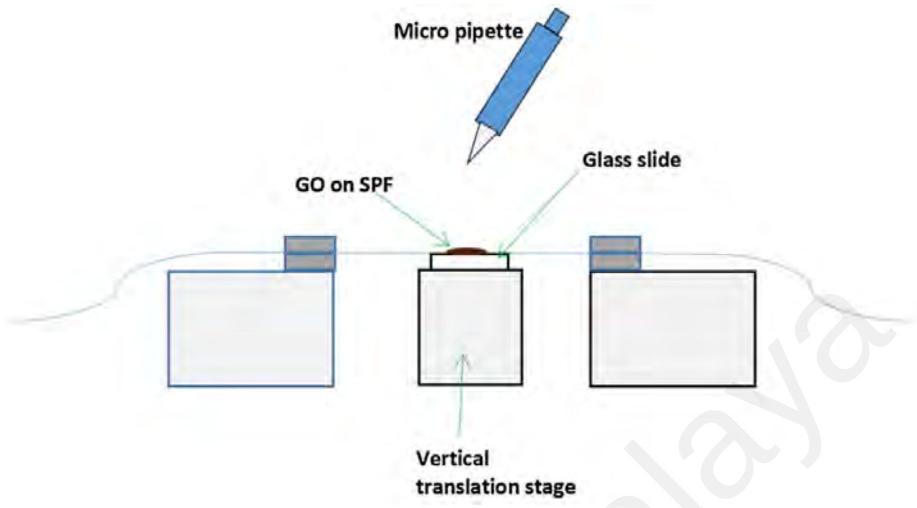

Figure 3.12: Deposition of Graphene oxide on SPF arrangement

The translation stage is moved vertically by adjusting the Newport SM-13 Vernier micrometer knob until the glass slide reaches the SPF surface at the bottom side. After that, GO with amount 2.5 μL was drop-cast on the SPF using 2.5 μL Eppendorf Research pipette. Figure 3.13 shows the drop-cast of GO on the SPF from the start session until the GO is dried. This procedure is carried out by transmission power real-time monitoring method whereby the ASE light source power is fixed to as low as of -27.5 dBm. This power of the signal is purposely set low to avoid any thermophoresis repulsion possibility as the GO nanoparticles are negatively charged in water solvent.

This happened because before the GO solution is drop-cast, the SPF is exposed and at the same time a substantial amount of light was leak out. The power of the signal measured is -27.5 dBm at this moment. After the GO was dropped, an artificial cladding around the corner is formed allowing more light trapped within the core. Thin film begins to form as the GO solution dries around the exposed core which can be depicted by the signal power rising.

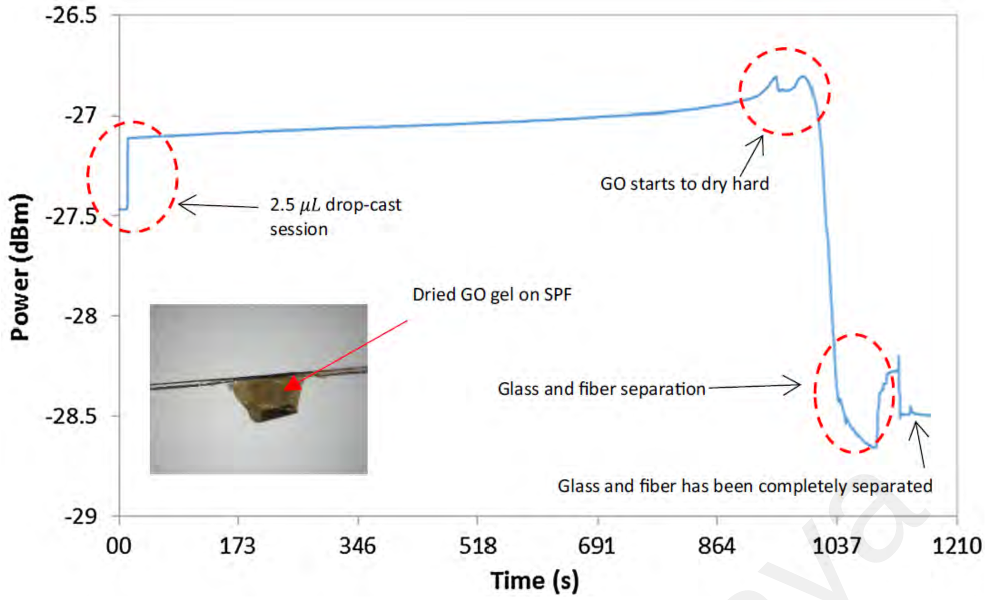

Figure 3.13: Real-time transmission power monitoring for deposition of GO solution on 1.8 dB insertion loss SPF

Nevertheless, when the thin film become harden around the exposed core, loss is produced as the GO molecules start to interact with signal propagate. The signal power initially drops from this moment. Then, the SPF is moved gently from the solid GO thin film and the power begins to stable. For this case, GO refractive index plays a crucial role as its refractive index is greater than the core which will strip away the power from the core. The inset in Figure 3.13 captured the microscopic image of GO that been deposited on SPF and have 3.02 dB and 3.71 of insertion loss and PDL respectively. The gap between the core and the polished surface is nearly 37.3 µm if the insertion loss is 1.5 dB and 4.63 µm if the insertion loss is 5.3 dB.

As for the bending characterization of SPF with GO coating, the steps was just same for previous section. According to Figure 3.14, the power able to recover after undergoing bending up to Δs = 200.0 µm. Power deviations are not observed for all Δs and it also observed that the transmission spectrum is identical to the SPF without GO coating.

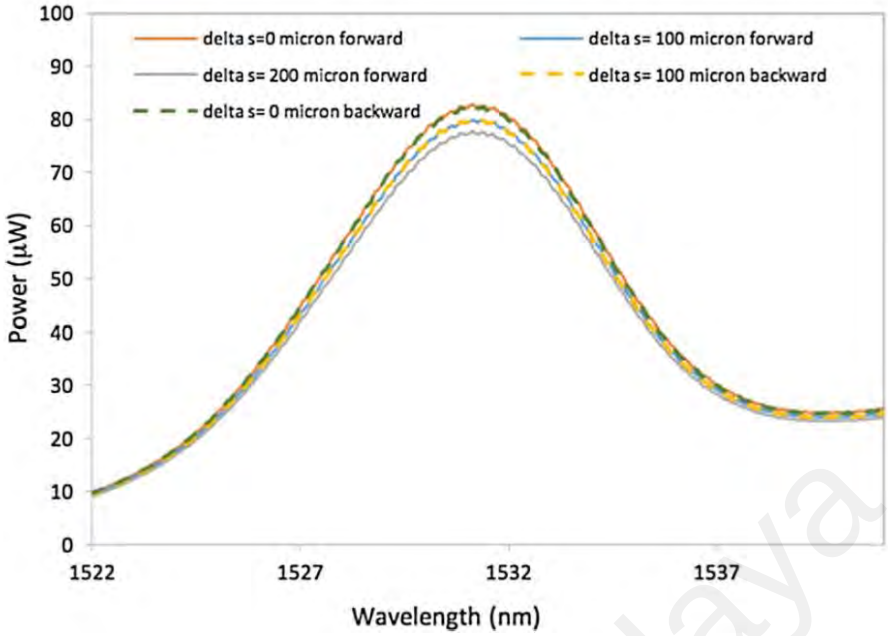

Figure 3.14: SPF ASE spectrum with GO deposited undergo bending forward and backward translation

Figure 3.15 depicts the ASE spectra for SPF deposited with GO solution bending up to Δs = 500.0 µm. The equivalent peak powers of the different Δs values are plotted in Figure 3.16. A linear graph is drawn with a slope of -0.0195 µW/µm and linearity of 0.9984.

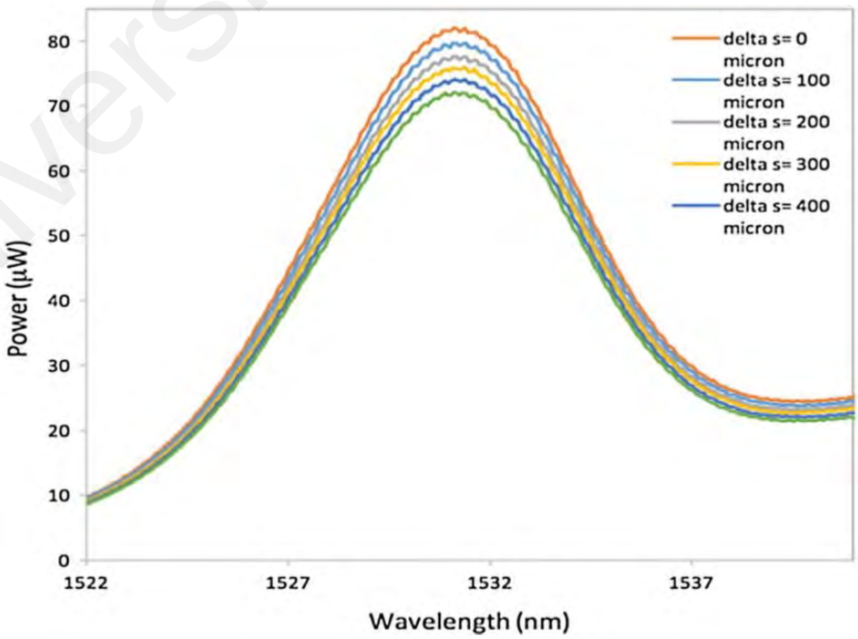

Figure 3.15: ASE spectra for SPF that deposited with GO at various bending displacement Δs = 0.0 to 500.0 µm

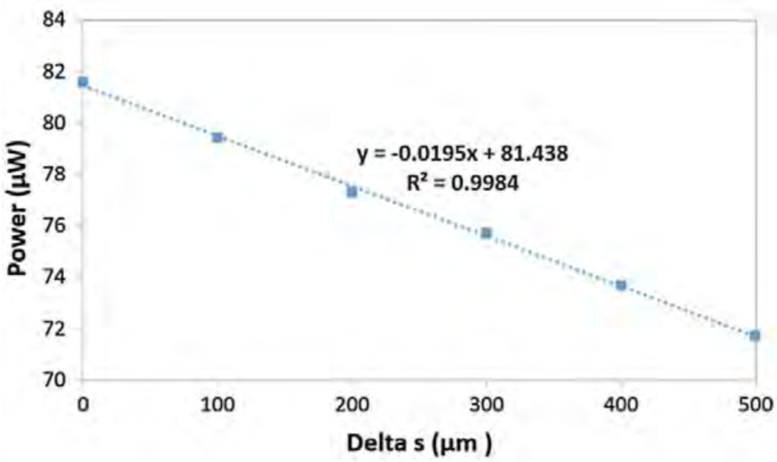

Figure 3.16: ASE spectra peak powers of SPF deposited GO at various bending displacement

The temperature change of SPF that have been coated with GO is plotted in Figure 3.17 and they were conducted in the same order to SPF without GO coating.

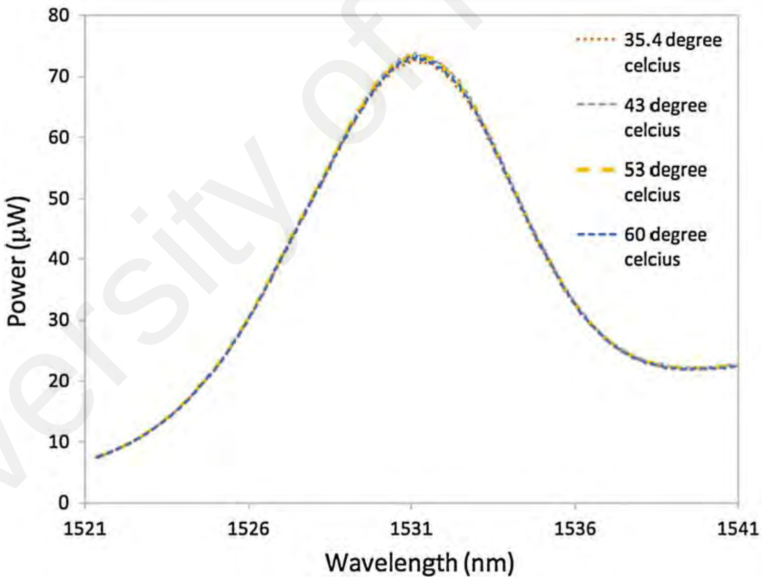

Figure 3.17: ASE spectra for SPF deposited GO at different temperature response

The ASE spectra were tested at various temperatures starts at 35.4 ºC up to 60.0 ºC. According to Figure 3.17, there is no significant change of spectral. Thus verifies that although GO is deposited, the SPF is resist to temperature change. This proved that the proposed SPF is suitable for sensing applications that require the measurement of strain independence from temperature.

In a nutshell, the characterization of SPF is done by testing the response of temperature and bending. Experimental results prove that the proposed SPF is very immune to temperature change. Furthermore, as for the bending test, the SPF able to recover the power when Δs reaches up to 200 μm displacement and returned back to 0 μm. As the Δs increase, spectral power reduces in a linear manner at different SPF insertion loss of 1.50, 5.27 and 12.39 dB. The identical test was also carried out with the deposition of GO on the surface of SPF. Similar output results can also be observed here. These results have verified that the fabricated SPFs are robust and their properties are insensitive towards bending and temperature changes, which make it very useful for various uses for example the generation of laser pulse, directional coupler and optical fiber sensor.

3.4 Molybdenum disulphide (MoS_2) and Carbon platinum (CPt) as Saturable Absorbers

Nowadays, transition metal dichalcogenides (TMD) has receives huge concern to be explored as one of the choices for saturable absorbers (SA). The TMD group build a structure in the form of X-M-X where a metal atom has been located between two chalcogen atom planes. They are adhered together by weak van der Waals force which makes this compound easy to exfoliate by ultrasonification in appropriate liquids (Coleman et al., 2011; May, Khan, Hughes, & Coleman, 2012). Besides that, TMD also more effective in absorbing and emitting photons because it has indirect semiconductor bandgap compare to other materials that exhibit the direct bandgap. For example, the material that has great interest lately is molybdenum disulphide (MoS_2). MoS_2 reflect the saturable absorption property better than graphene (K. Wang et al., 2013), has powerful linear optical response than graphene (Du et al., 2014; S. Wang et al., 2014) and also shows inferior saturation intensity as to graphene and carbon nanotubes (Sun, Popa, et al., 2010).

Meanwhile, Carbon platinum (CPt) is a recent material that used as SA. CPt may combine with SPF to operate as highly effective host platform that allows important interaction between light propagating through the SPF and SA surrounding it (Tien et al., 2008; Wagoner, McCallion, & Jameson, 1999). The fabrication of CPt-based SA is done by combining chloroplatinic acid hexahydrate ($H_2PtCl_6{\cdot}6H_2O$) with activated powdered carbon. Both compounds were gain from Sigma-Aldrich.

3.5 Non-linear absorption properties of MoS2 and CPt SAs

The balanced twin detector technique is shown in Figure 3.18. The configuration is carrying out to obtain the nonlinear characteristics of the MoS_2 and CPt as the SAs. The pulse-seed for the MoS_2 SA is acquired from a mode-locked fiber laser with a central wavelength of 1550 nm, pulse width of 0.70 ps and repetition rate of 28.7 MHz. Whereas, for the CPt SA, the central wavelength of the fiber laser operating is 1560 nm with the mode-locked output at a pulse width and repetition rate of 0.70 ps and 27.93 MHz respectively as the source signal for the measurement. The pulse seed is channel to a low-dispersion amplifier and variable optical attenuator before being split up by a 3-dB coupler. One output of the coupler is designated as the reference, and connected directly to a Thorlabs optical power meter (OPM), as depicted in Figure 3.18 while the other output is linked to the MoS_2 SA, which is connected to a second input of the OPM. The collected data is then inserted into Equation (3.1):

$$\alpha(I) = \frac{\alpha_s}{1+\frac{I}{I_{sat}}} + \alpha_{ns} \tag{3.1}$$

where α is absorption, I is intensity, α_s is saturable absorption, α_{ns} is non-saturable absorption and I_{sat} is saturation intensity.

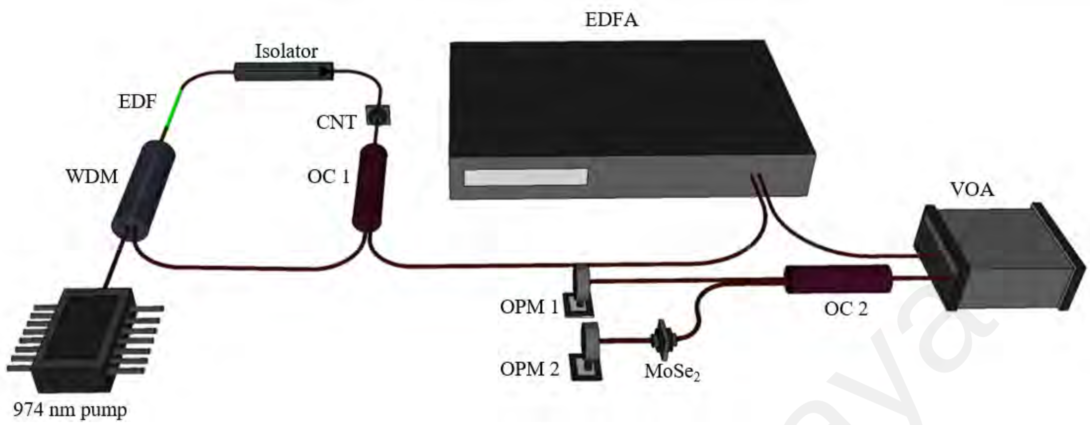

Figure 3.18: Balance twin detector technique configuration

The gained experimental result is plotted as in Figure 3.19. From the graphs, the obtained modulation depth value for MoS_2 was calculated at 7.7% and a saturation intensity of 0.002 MW/cm^2.

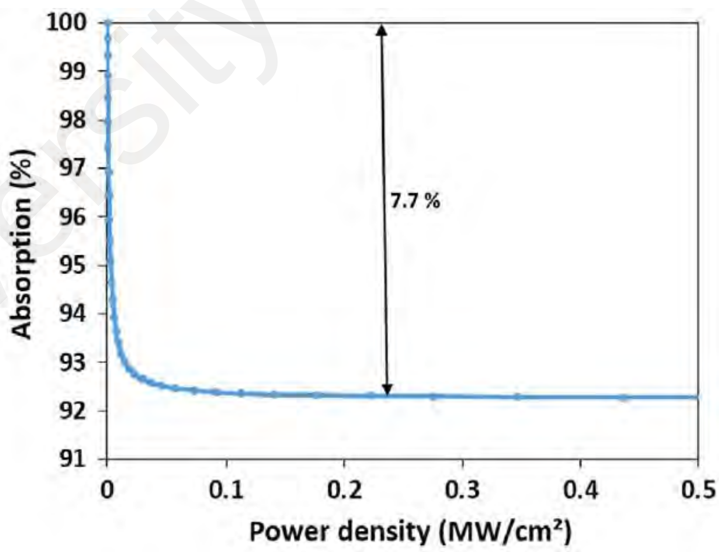

Figure 3.19: Modulation depth for MoS_2 saturable absorber

While for the CPt, the modulation depth and saturation intensity was figure out at 0.6% and 0.001 MW/cm^2 respectively as depicted in Figure 3.20. these value is considered as low compared to Chen et al., ranging from 10.74 to 342.6 MW/cm^2 (H. Chen et al., 2016; Y. Chen et al., 2015). It must be notify that the values obtained for materials for example tungsten disulfide based and black phosphorus based SAs are very optically active. SAs metal based such as Ag and Zn have much lower saturation intensities and modulation depths values 0.54 and 0.016 MW/cm^2 and 31.6% and 3.5%, respectively (H Ahmad, CSJ Lee, et al., 2016; H Ahmad, NE Ruslan, et al., 2016). This difference may due the dissimilar fabrication and preparation methods of the SA. Thus provides various quality of the SA and also the absorption of the edge states in the bandgap (Roxlo, Chianelli, Deckman, Ruppert, & Wong, 1987; Roxlo et al., 1986). However, although the saturation intensity in this research is lower compare to commonly used values, that might be advantageous for obtaining an output of pulse fiber laser (R. Woodward et al., 2014).

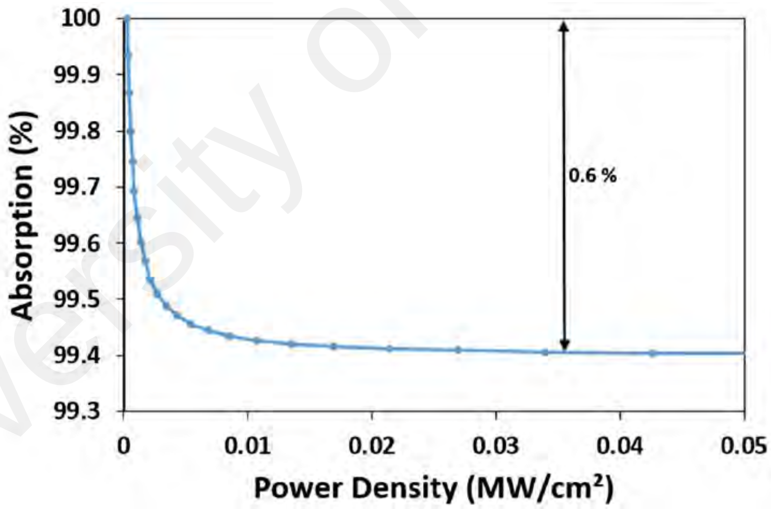

Figure 3.20: Modulation depth of CPt SA

The CPt-based SA was deposited by dropping 25 μL of the solution on the surface of SPF by employing micropipette and let it dried in air. The dry SPF CPt coating was then integrated into the laser resonator to generate Q-switched output.

CHAPTER 4: RESULT AND DISCUSSION

This chapter presents the performance of both Molybdenum disulfide and Carbon platinum SAs in generating Q-switching fiber laser. The SPF is in cooperated into the laser resonator role as wavelength selective element. The gained Q-switched spectrum is observed using optical spectrum analyzer (OSA) and the experimental result will be further explained in this section.

4.1 Performance of MoS_2 as Saturable Absorber in Generating Q-switched on Side-polished Fiber

The proposed experimental arrangement was noticed to obtain CW lasing at 11.6 mW and laser threshold at 14.8 mW pump power. In the region of Q-switching threshold, pulse having 14.1 kHz repetition rate and 0.6 mW output power is gained with 0.039 µJ of corresponding pulse energy. The maximum power for the Q-switching is 45.6 mW before the pulse starts to diminish.

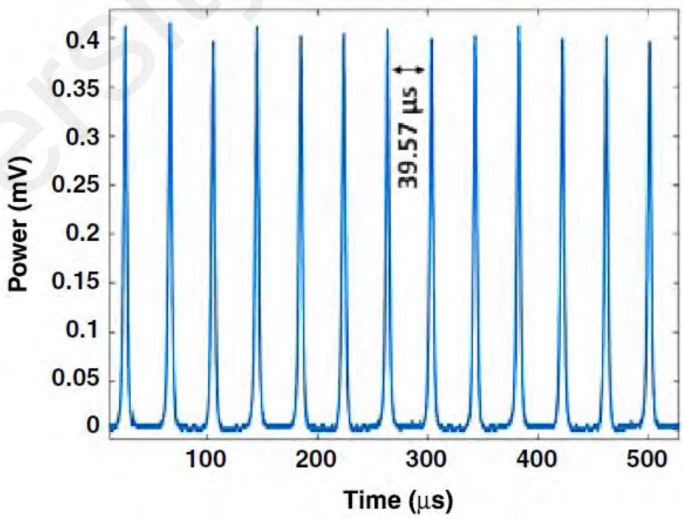

Figure 4.1: Q-switched pulse train at repetition rate of 25.27 kHz and pulse period of 39.57 µs

Figure 4.1 captured the pulse train achieved at the maximum pump power by the oscilloscope (OSC) with repetition rate of the pulse is 25.27 kHz and the pulse period of is 39.57 μs. By zooming into a single pulse explained that one pulses have an average full-width and half-maximum (FWHM) value of 3.19 μs. Microstructures can be seen throughout the pulse edge and it is referred to mode beating inside the pulses (Latiff et al., 2016). This is shown in Figure 4.2.

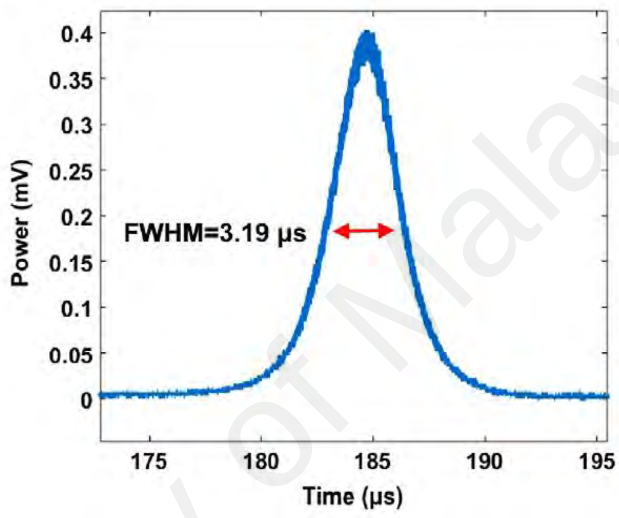

Figure 4.2: Single Q-switched pulse with 3.19 μs of FWHM

Figure 4.3 (a) depict the graphs of repetition rate and pulse width versus pump power. The obtained traces are same to common Q-switched laser when the repetition rate increasing as the pump power increase. Whereas, the pulse width drops when the pump power increases. The repetition rate and pulse width are 14.1 kHz and 7.9 μs respectively at the initial pump powerof 14.8 mW. The repetition rate seems to be inclines as the pump power increases until a maximum repetition rate of 25.27 kHz which is achieved at pump power of 45.6 mW. This shows no sign of deterioration or degradation which proves that the SA has not approached its damage threshold and would lie well above the maximum pump power available here (Richardson, Nilsson, & Clarkson, 2010). Apart from that, the pulse width decrease slightly from its initial value to about 5.1 μs at a pump power of 21.2 mW and continues to decrese as the pump power increases although to a lower rate of 3.19 μs at a pump power of 45.6 mW.

Besides that, Figure 4.3(b) plotted the average output power and pulse energy also linearly increase when increasing pump power. The average output power and pulse energy have values of 0.6 mW and 0.04 μJ at an initial pump power of 14.8 mW. At the maximum pump power of 45.6 mW, the observed average output power and pulse energy are 2.27 mW and 0.09 μJ respectively. This again corresponds with the behavior expected of a *Q*-switched laser (Degnan, 1995). It is important to note that even at the maximum pump power, no instability is observed in the previous mentioned parameters indicate that the fiber laser is still operate below the thermal damage threshold of the SA.

This verifies by turning down the pump power from the maximum to threshold value and it was seen that the measured parameters match closely to the readings achieved when the pump power is increased gently. Moreover, observation of the pulses for more than 6 hours duration shows no significant changes. Thus proves that the laser is highly stable.

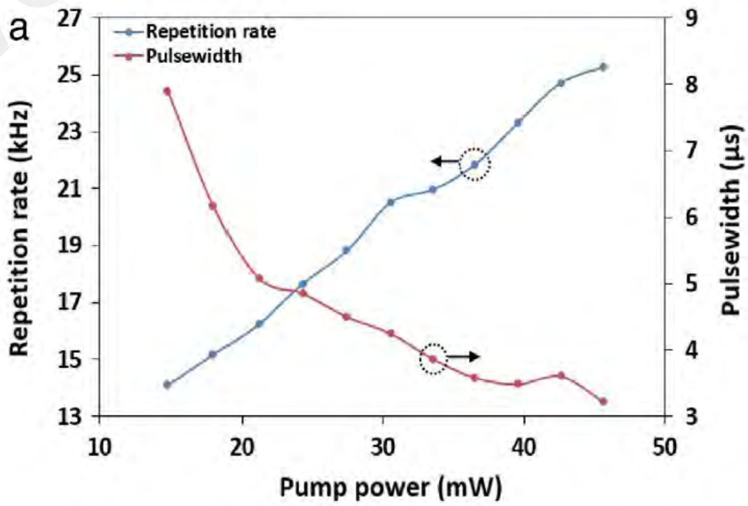

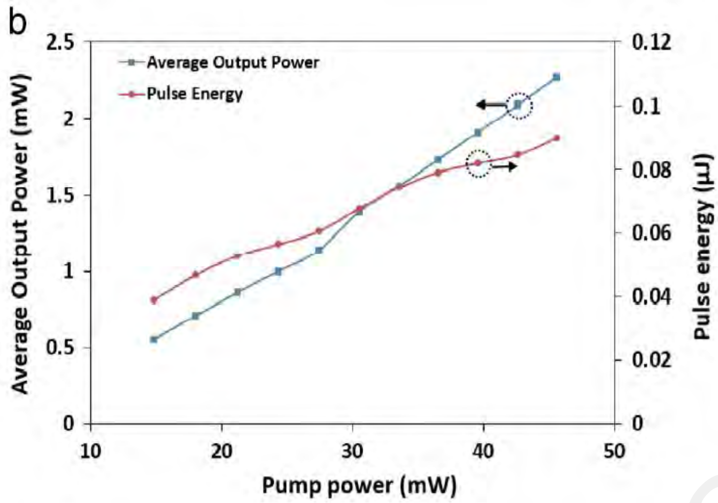

Figure 4.3: (a) Repetition rate and pulse width and (b) average output power and pulse energy against increasing pump power.

The summarized output gained by the configuration with and without the SA employment is plotted as Figure 4.4. It can be obeserved that without the SA integrated, a peak of single output at 1558 nm is achieved with a substantially narrow FWHM of 0.1 nm. The peak is well defined, with a peak power of about −15.4 dBm and a peak-to-floor value of 21.6 dB. By inserting the SA, in the peak wavelength seen to be widen significantly with 3-dB value around 1.9 nm. The rise in the peak wavelength of about 3 nm from its previous value of 1558 nm is a result of the lasing wavelength moving toward a region of higher gain to compensate for the additional losses induced by the insertion of the SA into the laser cavity (Harun et al., 2012). The new peak wavelength is measured to be 1561.5 nm with a peak intensity value of −15.4 dB. Given a peak-to-floor ratio of around 37.8 dB thus can be verified that the MoS_2 plays a crucial role in generating the *Q*-switched output. The removal of MoS_2 based SA will result in continuous wave output only.

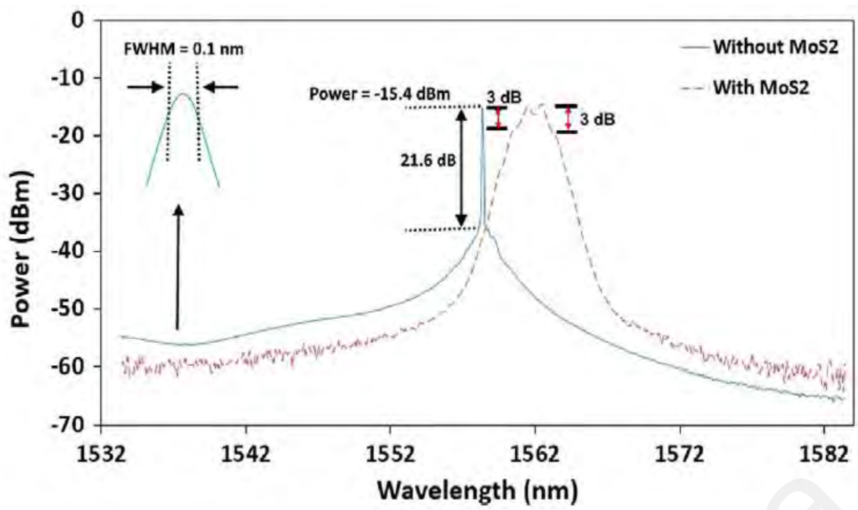

Figure 4.4: The laser spectra for SPF without MoS_2 (solid line), with 0.2 nm of 3-dB value and MoS_2 saturable absorber (dotted line) with 1.9 nm of 3-dB value

When comparing to other SA materials, MoS_2 shows a somewhat comparable performance. The comparison of MoS_2 based SA performance is summarized in Table 4.1. It can be said that the repetition rate and pulse width of the MoS_2 based SA performance is comparable to the $MoSe_2$ based SA. This is not surprising as both materials are transition metal dichalcogenides and thus would behave identically. Higher repetition rates of almost 4 times higher can be achieved for pulses generated by MoS_2 and $MoSe_2$ based SAs, depending on the configuration of the laser cavity. Similarly, when compared to graphene, the performance of these SAs is also similar, with graphene based SAs able to generate pulses at output rates of similar repetition rates and pulse widths. However, it must be taken into account that graphene can be more involved to fabricate and thus costly, and there have also been numerous reports of *Q*-switched graphene SAs. Overall, it can be seen that the MoS2 based SA performs better than those formed by other SA materials, and carries the advantage of lower cost and easier fabrication as compared to SA materials such as graphene, black phosphorous and silver. The low pulse energy obtained in this work can be attributed to losses due to the leakage of light from the D-shaped fiber.

Table 4.1: Difference of SA material performance parameter

SA material	Repetition rate (kHz)	Min. pulse width (μs)	Max. pulse energy (nJ)	Reference
$MoSe_2$	32.8	30.4	57.9	(Ahmad, Suthaskumar, Tiu, Zarei, & Harun, 2016)
MoS_2	101.17	1.4	-	(Harith Ahmad et al., 2016)
	25.27	3.19	0.09	[this work]
Graphene	53.2	3.2	17.41	(LQ Zhang, Zhuo, Wang, & Wang, 2012)
CNT	16.1	11.6	90.3	(Harun et al., 2012)
Ag	58.5	2.4	132	(Guo et al., 2016)
Bi_2Te_3	1.2	1.21	NA	(C. Zhao et al., 2012)
BP	15.8	10.3	94.3	(Y. Chen et al., 2015)

Note: $MoSe_2$: Molybdenum diselenide, CNT: Carbon nanotubes, Ag: Silver, Bi_2Te_3: Bismuth telluride, BP: Black phosphorus

The proposed system is highly robust and easy to fabricate, making it highly advantageous for a variety of real-world applications. The proposed laser can find numerous applications in areas such as telecommunications, manufacturing, medicine and sensing (Leondes, 2007), and provides a robust yet cost-effective platform that can easily accommodate various other 2-D and 3-D materials for SA applications.

4.2 Performance of CPt as Saturable Absorber in Generating Q-switching on Side-polished Fiber

The lasing spectrum of the proposed Q-switched laser is obtained using a Yokogawa AQ6370B optical spectrum analyzer (OSA) with a resolution of 0.02 nm. Lasing is observed to occur at a pump power of 120.0 mW, while Q-switching begins at a pump power of 135.5 mW. Figure 4.5 shows an ordinary optical output spectrum of the Q-switched pulse at a pump power of 135.5 mW, which has a central wavelength at approximately 1559.34 nm and a 3-dB bandwidth of 1.2 nm.

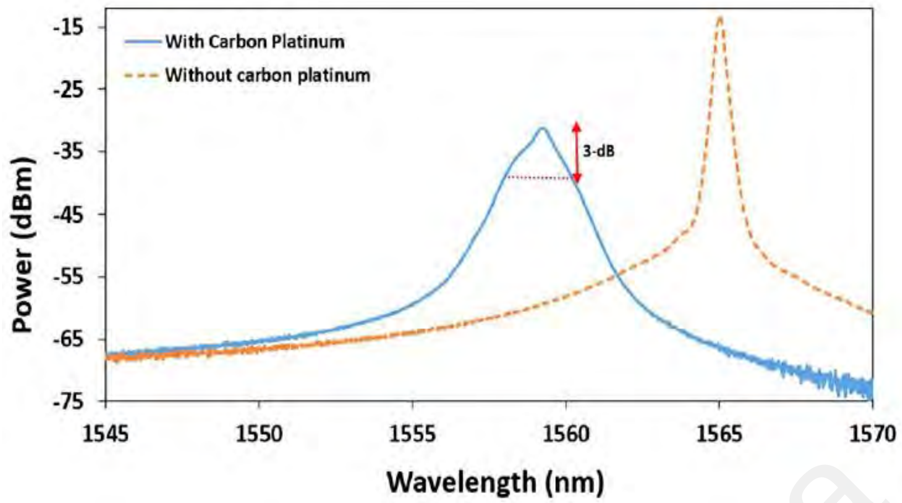

Figure 4.5: Output spectrum with and without CPt SA

Figure 4.6 (a) provides the pulse train generated by the Q-switched fiber laser. The pulse train can be seen to have a repetition rate of 99.6 kHz at a pump power of 179.6 mW. The pulses are spaced 0.1 μs apart, with each individual pulse having a full width at half-maximum (FWHM) of 1.5 μs. This is given in Figure 4.6 (b). It can also be seen from the figure that the pulse is smooth, with a clean Sech2-shape and no Kelly's sidebands observed, thereby eliminating the possibility of a mode-locked pulse.

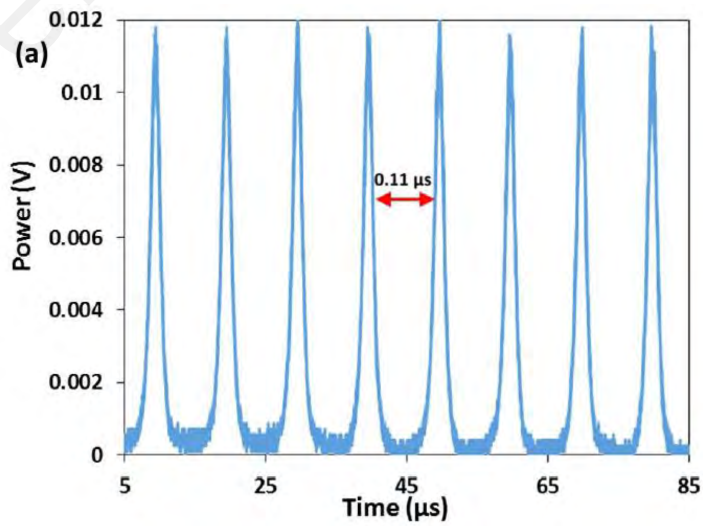

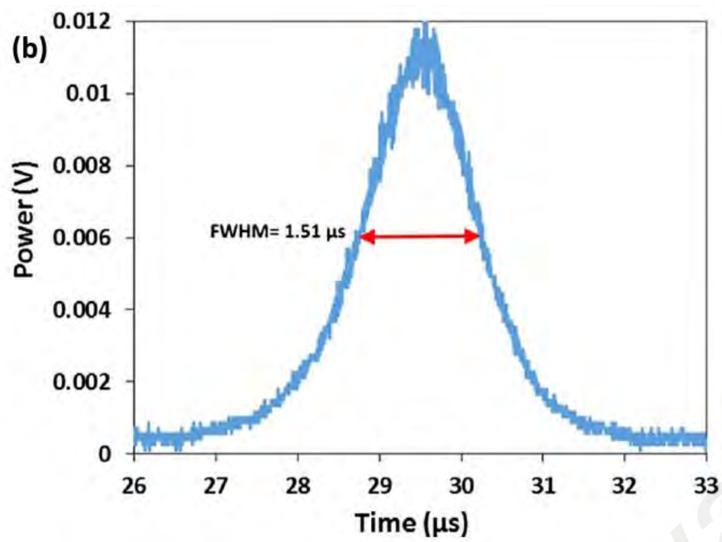

Figure 4.6: (a) Pulse train at 179.6 mW pump power and (b) single-pulse capture at the same pump power

When observed against a rising pump power, the repetition rate, pulse width, pulse energy and average output power of the output generated by the proposed system corresponds to that of a typical Q-switched laser (Popa et al., 2011). For the proposed system, the repetition rate is approximately 67.4 kHz at a pump power of 135.5 mW, with a pulse width, pulse energy, and average output power of 2.3 μs, 5.2 nJ, and 0.35 mW, respectively, at the same pump power. As the pump power increases, reaching a value of 230.0 mW, the pulse energy, average output power, and repetition rate are all seen to increase in an almost linear fashion to 5.8 nJ, 0.76 mW, and 131.6 kHz respectively. The pulse width, on the other hand, decreases reaching a minimum value of 1.02 μs at the maximum pump power.

Although the pulse width is typically expected to decrease exponentially as the pump power rises, the gradual linear decrease observed in this work is attributed to the SAs saturation limit being much higher than that can be reached by the system. It is expected that should the pump power be increased further, the pulse width would eventually plateau out before reaching its saturation value and remain unchanged even if the pump power continues to be increased (Davis, Digonnet, & Pantell, 1998; Ganiel, Hardy, & Treves, 1976).

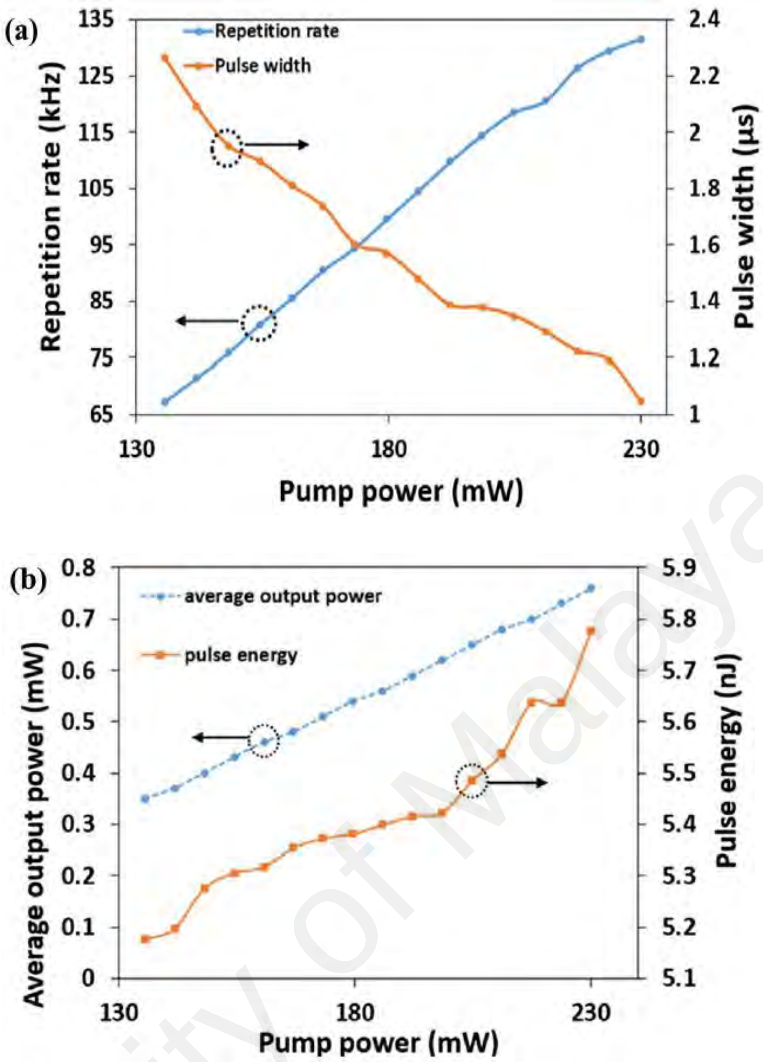

Figure 4.7: (a) Repetition rate and pulse width against the pump power and (b) the average output power and pulse energy against the pump power

The response of the repetition rate and pulse width against the pump power is given in Figure 4.7 (a), while the response of the pulse energy and average output power against the pump power is given in Figure 4.7 (b). The relatively high repetition rate can be achieved due to the low saturable optical intensity of the SA (Tang et al., 2013; Yu et al., 2014). The repetition rate achieved in this work is substantially higher than that typically observed, ranging from a few kHz to 100 kHz (Álvarez-Tamayo et al., 2016), and it is also possible to achieve higher repetition rates should higher pump powers be available.

Figure 4.8 provides the radio-frequency (RF) scan of the generated pulses. From the figure, it can be observed that a single fundamental frequency is obtained, corresponding to a repetition rate of 131.56 kHz taken at a pump power of 230 mW. A signal-to-noise ratio (SNR) of 49.62 dB is observed, indicating a highly stable pulse. The inset of the figure shows the RF harmonics taken from a bigger span of 100 kHz at pump power of 230 mW.

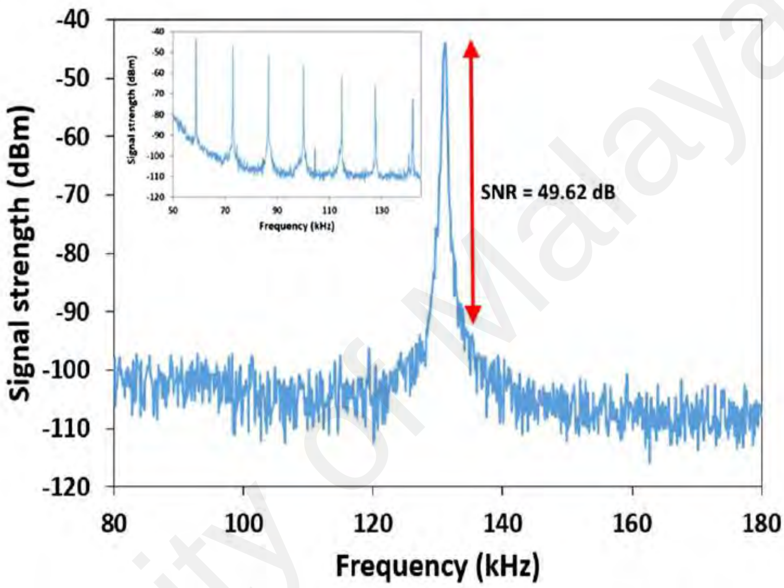

Figure 4.8: RF optical spectrum and inset showing the wideband RF spectrum

An SPF deposited with CPt saturable was demonstrated to get a Q-switching pulse. The SPF is made by using a fabrication process that is very effective and affordable compared to commercial SPF. A micropipette is used to drop the CPt on the surface of the SPF. A rigid Q-switched pulse at a central wavelength of 1559.34 nm and SNR of 49.62 dB is generated by integrating the SPF into the proposed laser resonator.

The maximum repetition rate is 131.6 kHz, having an average output power of 0.76 mW with pulse energy of 5.8 nJ and a pulse width of 1.02 μs taken at a pump power of 230.0 mW. This result demonstrates that this SPF and the CPt SA are capable of producing a Q-switched fiber laser, which will be very significant in many fiber laser and sensor applications, especially those that need cheap, compact, and effective optical equipment.

CHAPTER 5: CONCLUSION

5.1 Conclusion

The motivation of this research is lack of research on side-polished fiber (SPF) in generating fiber laser by using 2D materials such as Molybdenum disulfide (MoS_2) and Carbon platinum (CPt) as saturable absorbers. There are many saturable absorbers demonstrated by other researchers, but less focus on SPF. If the SPF works as expected in the proposed experimental set-up, it will open many more possibilities of applying SPF in fiber lasers generation. Hence, wider options will available and might be important for the industrial applications.

In the introductory of this research, the SPF is implemented by using cost-effective and high efficient method. The SPF is fabricated by employing single-mode fiber (SMF-28), polishing wheel, silicon carbide paper and 5 V DC motor as the basic requirements of the process. Firstly, the fiber coating of SMF-28 is stripped and it then suspended over the polishing wheel after cleans with alcohol to remove the dirt and polymer debris. After that, the uncoated SMF-28 is assembling along the fiber holders in the polishing set-up. The voltage of the motor is increase slowly to start the process. When the red light supply by fault locator can be seen from the stripped part of the fiber, the motor speed is slowly decreased to prevent from over-polished. Usually the process takes around 15 minutes to produce one SPF.

Apart from that, the SPF is then characterized by testing its strength via bending and temperature change. The characterization process is also repeated by dropping Graphene oxide (GO) on the surface of SPF and again test the effect with temperature and bending. Firstly, to create the bending condition, one translation stage remains fixed in position while the other one moves horizontally. The displacement is widening from 0.00 to 200 μm. The output measurement shows the ability of the SPF to maintain its power transmission characteristics before and after undergoing the bending. Moreover, for temperature testing, three samples of SPFs with different insertion losses are placed on a hotplate to provide heat below the glass slide which temperature change from 27 ºC to 60 ºC. The result shows no significant spectrum change which verifies that our fabricated SPFs are robust to temperature noise.

Last but not least, to study in depth about the SPF performance, two types of saturable absorbers (SAs) are used to generate passive Q-switched fiber laser. The laser cavity set-up is using EDF as the gain medium and the materials employed are Molybdenum disulphide (MoS_2) and Carbon platinum (CPt).

From the research, by employing MoS_2 material, the purposed laser has a Q-switching threshold of 14.8 mW and able to generate pulse output with a repetition rate and pulse width of up to 25.27 kHz and 3.19 μs respectively. The maximum pump power is 45.6 mW with average output power and pulse energy of 2.26 mW and 0.09 μJ. The pulse have an average signal-to-noise ratio of 37.8 dB which indicates a stable output and making the purposed laser highly suited for variety of sensor, communications and industrial applications. Whereas for CPt material, a stable Q-switched spectrum can be seen at 1559.34 nm with repetition rate and pulse width of 99.6 kHz and 0.11 μs at 179.6 mW pump power. A signal-to-noise ratio of 49.62 dB shows that the Q-switched pulse is highly stable.

5.2 Recommendation

For further improvement, several aspects need to be considered for instance the fabrication of SPF. SPF can be manipulated and focused on various diameter, depth, length and surface roughness. By varying the parameters of SPFs, it will enhance the ability to control the properties of mode-interference and wavelength selective characteristic. Nowadays, most of the research is concentrating on the usage of fiber

Bragg grating (FBG) and less attention on SPF in laser application. It would be more interesting to explore the fabrication of SPF for further investigation in performance of Q-switching operation with new SA materials that able to produce Q-switching in various region.

REFERENCES

Abedin, K., Taunay, T., Fishteyn, M., Yan, M., Zhu, B., Fini, J., . . . Wisk, P. (2011). Amplification and noise properties of an erbium-doped multicore fiber amplifier. *Optics express, 19*(17), 16715-16721.

Ahmad, H., Amiri, I., Zulkifli, A., Hassan, H., Safaei, R., & Thambiratnam, K. (2017). Stable dual-wavelength erbium-doped fiber laser using novel fabricated side-polished arc-shaped fiber with deposited ZnO nanoparticles. *Chinese Optics Letters, 15*(1), 011403.

Ahmad, H., Faruki, M., Razak, M., Jaddoa, M., Azzuhri, S., Rahman, M., & Ismail, M. (2017). A combination of tapered fibre and polarization controller in generating highly stable and tunable dual-wavelength C-band laser. *Journal of Modern Optics, 64*(7), 709-715.

Ahmad, H., Ismail, M. A., Suthaskumar, M., Tiu, Z. C., Harun, S. W., Zulkifli, M. Z., . . . Sivaraj, S. (2016). S-band Q-switched fiber laser using molybdenum disulfide (MoS2) saturable absorber. *Laser Physics Letters, 13*(3), 035103.

Ahmad, H., Lee, C., Ismail, M., Ali, Z., Reduan, S., Ruslan, N., . . . Harun, S. (2016). Zinc oxide (ZnO) nanoparticles as saturable absorber in passively Q-switched fiber laser. *Optics Communications, 381*, 72-76.

Ahmad, H., Ruslan, N., Ali, Z., Reduan, S., Lee, C., Shaharuddin, R., . . . Ismail, M. (2016). Ag-nanoparticle as a Q switched device for tunable C-band fiber laser. *Optics Communications, 381*, 85-90.

Ahmad, H., Suthaskumar, M., Tiu, Z., Zarei, A., & Harun, S. (2016). Q-switched Erbium-doped fiber laser using MoSe 2 as saturable absorber. *Optics & Laser Technology, 79*, 20-23.

Álvarez-Tamayo, R. I., Durán-Sánchez, M., Pottiez, O., Ibarra-Escamilla, B., Kuzin, E. A., & Espinosa-Martínez, M. (2016). Active Q-switched Fiber Lasers with Single and Dualwavelength Operation *Fiber Laser*: InTech.

Amiri, I., Ariannejad, M., & Ahmad, H. (2016). Tunable multi-wavelength generation using InGaAsP/InP microring resonator with detectable resonance wavelength shift due to a sensing cladding section. *Chinese Journal of Physics, 54*(5), 780-787.

Baker, C. C., Friebele, E. J., Burdett, A. A., Rhonehouse, D. L., Fontana, J., Kim, W., . . . Zhang, J. (2017). Nanoparticle doping for high power fiber lasers at eye-safer wavelengths. *Optics express, 25*(12), 13903-13915.

Bao, Q., Zhang, H., Wang, Y., Ni, Z., Yan, Y., Shen, Z. X., . . . Tang, D. Y. (2009). Atomic-layer graphene as a saturable absorber for ultrafast pulsed lasers. *Advanced Functional Materials, 19*(19), 3077-3083.

Basharin, A. A., Chuguevsky, V., Volsky, N., Kafesaki, M., & Economou, E. N. (2017). Extremely high Q-factor metamaterials due to anapole excitation. *Physical Review B, 95*(3), 035104.

Bergh, R., Kotler, G., & Shaw, H. (1980). Single-mode fibre optic directional coupler. *Electronics Letters, 16*(7), 260-261.

Biagi, E., Margheri, F., & Menichelli, D. (2001). Efficient laser-ultrasound generation by using heavily absorbing films as targets. *ieee transactions on ultrasonics, ferroelectrics, and frequency control, 48*(6), 1669-1680.

Bilro, L., Alberto, N., Sá, L. M., de Lemos Pinto, J., & Nogueira, R. (2011). Analytical analysis of side-polished plastic optical fiber as curvature and refractive index sensor. *Journal of lightwave technology, 29*(6), 864-870.

Bonaccorso, F., Sun, Z., Hasan, T., & Ferrari, A. (2010). Graphene photonics and optoelectronics. *Nature photonics, 4*(9), 611.

Boscolo, S., & Finot, C. (2017). *Shaping light in nonlinear optical fibers*: John Wiley & Sons.

Chen, C.-M., Lee, Y.-W., Huang, C.-W., Chen, S.-K., & Jiang, J.-r. (2018). Passively q-switched fiber laser system and method for fabricating a saturable absorber of the system: Google Patents.

Chen, H., Chen, Y., Yin, J., Zhang, X., Guo, T., & Yan, P. (2016). High-damage-resistant tungsten disulfide saturable absorber mirror for passively Q-switched fiber laser. *Optics express, 24*(15), 16287-16296.

Chen, X., Zhang, W., Liu, C., Hong, Y., & Webb, D. J. (2015). Enhancing the humidity response time of polymer optical fiber Bragg grating by using laser micromachining. *Optics express, 23*(20), 25942-25949.

Chen, Y., Jiang, G., Chen, S., Guo, Z., Yu, X., Zhao, C., . . . Tang, D. (2015). Mechanically exfoliated black phosphorus as a new saturable absorber for both Q-switching and mode-locking laser operation. *Optics express, 23*(10), 12823-12833.

Coelho, L., de Almeida, J., Santos, J., Ferreira, R., André, P., & Viegas, D. (2015). Sensing structure based on surface plasmon resonance in chemically etched single mode optical fibres. *Plasmonics, 10*(2), 319-327.

Coleman, J. N., Lotya, M., O'Neill, A., Bergin, S. D., King, P. J., Khan, U., . . . Smith, R. J. (2011). Two-dimensional nanosheets produced by liquid exfoliation of layered materials. *Science, 331*(6017), 568-571.

Cordaro, M., Rode, D. L., Barry, T., & Krchnavek, R. R. (1994). Precision fabrication of D-shaped single-mode optical fibers by in situ monitoring. *Journal of lightwave technology, 12*(9), 1524-1531.

Davis, M., Digonnet, M., & Pantell, R. H. (1998). Thermal effects in doped fibers. *Journal of lightwave technology, 16*(6), 1013.

Degnan, J. J. (1995). Optimization of passively Q-switched lasers. *IEEE journal of quantum electronics, 31*(11), 1890-1901.

Delgado-Pinar, M., Zalvidea, D., Diez, A., Pérez-Millán, P., & Andres, M. (2006). Q-switching of an all-fiber laser by acousto-optic modulation of a fiber Bragg grating. *Optics Express, 14*(3), 1106-1112.

Denker, B., Galagan, B., Sverchkov, S., & Prokhorov, A. (2013). Erbium (Er) glass lasers *Handbook of Solid-State Lasers* (pp. 341-358): Elsevier.

Dong, L., & Peng, X. (2015). Rare earth doped and large effective area optical fibers for fiber lasers and amplifiers: Google Patents.

Du, J., Wang, Q., Jiang, G., Xu, C., Zhao, C., Xiang, Y., . . . Zhang, H. (2014). Ytterbium-doped fiber laser passively mode locked by few-layer Molybdenum Disulfide (MoS 2) saturable absorber functioned with evanescent field interaction. *Scientific reports, 4*, 6346.

Eda, G., & Maier, S. A. (2013). Two-dimensional crystals: managing light for optoelectronics. *ACS nano, 7*(7), 5660-5665.

Eickhoff, W. (1980). In-line fibre-optic polariser. *Electronics Letters, 16*(20), 762-764.

Esmaeilzadeh, H., Arzi, E., Légaré, F., Rivard, M., & Hassani, A. (2015). A super continuum characterized high-precision SPR fiber optic sensor for refractometry. *Sensors and Actuators A: Physical, 229*, 8-14.

Fermann, M. E., & Hartl, I. (2013). Ultrafast fibre lasers. *Nature photonics, 7*(11), 868-874.

Ganiel, U., Hardy, A., & Treves, D. (1976). Analysis of injection locking in pulsed dye laser systems. *IEEE journal of quantum electronics, 12*(11), 704-716.

Gattass, R. R., & Mazur, E. (2008). Femtosecond laser micromachining in transparent materials. *Nature photonics, 2*(4), 219.

Gattass, R. R., Sanghera, J. S., & Shaw, L. B. (2017). Compact infrared broadband source: Google Patents.

Geim, A. K., & Grigorieva, I. V. (2013). Van der Waals heterostructures. *nature, 499*(7459), 419.

Glass, A. M., DiGiovanni, D. J., Strasser, T. A., Stentz, A. J., Slusher, R. E., White, A. E., . . . Eggleton, B. J. (2000). Advances in fiber optics. *Bell Labs Technical Journal, 5*(1), 168-187.

Gloge, D. (1971). Weakly guiding fibers. *Applied optics, 10*(10), 2252-2258.

Guo, H., Feng, M., Song, F., Li, H., Ren, A., Wei, X., . . . Tian, J. (2016). $ Q $-Switched Erbium-Doped Fiber Laser Based on Silver Nanoparticles as a Saturable Absorber. *IEEE Photonics Technology Letters, 28*(2), 135-138.

Harun, S., Ismail, M., Ahmad, F., Ismail, M., Nor, R., Zulkepely, N., & Ahmad, H. (2012). A Q-switched erbium-doped fiber laser with a carbon nanotube based saturable absorber. *Chinese Physics Letters, 29*(11), 114202.

Hussey, C., & Minelly, J. (1988). Optical fibre polishing with a motor-driven polishing wheel. *Electronics Letters, 24*(13), 805-807.

Ippen, E., Shank, C., & Dienes, A. (1972). Passive mode locking of the cw dye laser. *Applied Physics Letters, 21*(8), 348-350.

Jadidi, M. M., Kö ig-Otto, J. C., Winnerl, S., Sushkov, A. B., Drew, H. D., Murphy, T. E., & Mittendorff, M. (2016). Nonlinear terahertz absorption of graphene plasmons. *Nano letters, 16*(4), 2734-2738.

Jung, M., Koo, J., Debnath, P., Song, Y.-W., & Lee, J. H. (2012). A mode-locked 1.91 μm fiber laser based on interaction between graphene oxide and evanescent field. *Applied Physics Express, 5*(11), 112702.

Kashiwagi, K., & Yamashita, S. (2009). Deposition of carbon nanotubes around microfiber via evanascent light. *Optics express, 17*(20), 18364-18370.

Keller, U. (2003). Recent developments in compact ultrafast lasers. *nature, 424*(6950), 831.

Kienel, M., Müller, M., Klenke, A., Limpert, J., & Tünnermann, A. (2016). 12 mJ kW-class ultrafast fiber laser system using multidimensional coherent pulse addition. *Optics letters, 41*(14), 3343-3346.

Klenke, A., Hädrich, S., Eidam, T., Rothhardt, J., Kienel, M., Demmler, S., . . . Tünnermann, A. (2014). 22 GW peak-power fiber chirped-pulse-amplification system. *Optics letters, 39*(24), 6875-6878.

Knight, J., Birks, T., Russell, P. S. J., & Atkin, D. (1996). All-silica single-mode optical fiber with photonic crystal cladding. *Optics letters, 21*(19), 1547-1549.

Knight, J. C. (2003). Photonic crystal fibres. *nature, 424*(6950), 847.

Kogelnik, H. (1988). Theory of optical waveguides in book Guided wave optoelectronics edited by T. Tamir: Springer-Verlag, Berlin.

Kowalczyk, M., Bogusławski, J., Zybała, R., Mars, K., Mikuła, A., Soboń, G., & Sotor, J. (2016). Sb 2 Te 3-deposited D-shaped fiber as a saturable absorber for mode-locked Yb-doped fiber lasers. *Optical Materials Express, 6*(7), 2273-2282.

Kuan, W.-H., Kao, L.-T., Wang, J.-Y., & Lin, K.-H. (2018). Femto/nano-second switchable passively mode-locked fiber laser with analytic modeling by the cubic-quintic Ginzburg–Landau equation. *Optics letters, 43*(2), 341-344.

Kurkjian, C. R., Krause, J. T., & Matthewson, M. J. (1989). Strength and fatigue of silica optical fibers. *Journal of lightwave technology, 7*(9), 1360-1370.

Lancaster, D., Stevens, V., Michaud-Belleau, V., Gross, S., Fuerbach, A., & Monro, T. (2015). Holmium-doped 2.1 μm waveguide chip laser with an output power> 1 W. *Optics express, 23*(25), 32664-32670.

Latiff, A., Shamsudin, H., Aziz, N., Hashim, A., Irawati, N., Ahmad, H., & Harun, S. (2016). Mode-locked generation in thulium-doped fiber linear cavity laser. *Optik-International Journal for Light and Electron Optics, 127*(23), 11119-11123.

Lee, E. J., Choi, S. Y., Jeong, H., Park, N. H., Yim, W., Kim, M. H., . . . Kim, S. J. (2015). Active control of all-fibre graphene devices with electrical gating. *Nature communications, 6*, 6851.

Lee, J., Koo, J., Debnath, P., Song, Y., & Lee, J. (2013). A Q-switched, mode-locked fiber laser using a graphene oxide-based polarization sensitive saturable absorber. *Laser Physics Letters, 10*(3), 035103.

Lee, J., Koo, J., Jhon, Y. M., & Lee, J. H. (2014). A femtosecond pulse erbium fiber laser incorporating a saturable absorber based on bulk-structured Bi 2 Te 3 topological insulator. *Optics express, 22*(5), 6165-6173.

Leite, I. T., Turtaev, S., Jiang, X., Šiler, M., Cuschieri, A., Russell, P. S. J., & Čižmár, T. (2018). Three-dimensional holographic optical manipulation through a high-numerical-aperture soft-glass multimode fibre. *Nature photonics, 12*(1), 33.

Leondes, C. T. (2007). *Mems/nems:(1) handbook techniques and applications design methods,(2) fabrication techniques,(3) manufacturing methods,(4) sensors and actuators,(5) medical applications and MOEMS*: Springer Science & Business Media.

Lin, Y.-H., Lin, S.-F., Chi, Y.-C., Wu, C.-L., Cheng, C.-H., Tseng, W.-H., . . . Lin, G.-R. (2015). Using n-and p-type Bi2Te3 topological insulator nanoparticles to enable controlled femtosecond mode-locking of fiber lasers. *Acs Photonics, 2*(4), 481-490.

Liu, H., Chow, K., Yamashita, S., & Set, S. (2013). Carbon-nanotube-based passively Q-switched fiber laser for high energy pulse generation. *Optics & Laser Technology, 45*, 713-716.

Liu, L., Zheng, Z., Zhao, X., Sun, S., Bian, Y., Su, Y., . . . Zhu, J. (2013). Dual-wavelength passively Q-switched Erbium doped fiber laser based on an SWNT saturable absorber. *Optics Communications, 294*, 267-270.

Lü, X., Han, Q., Liu, T., Chen, Y., & Ren, K. (2014). Actively Q-switched erbium-doped fiber ring laser with a nanosecond ceramic optical switch. *Laser Physics, 24*(11), 115102.

Luo, Z., Wang, J., Zhou, M., Xu, H., Cai, Z., & Ye, C. (2012). Multiwavelength mode-locked erbium-doped fiber laser based on the interaction of graphene and fiber-taper evanescent field. *Laser Physics Letters, 9*(3), 229.

Luo, Z., Zhou, M., Weng, J., Huang, G., Xu, H., Ye, C., & Cai, Z. (2010). Graphene-based passively Q-switched dual-wavelength erbium-doped fiber laser. *Optics letters, 35*(21), 3709-3711.

Maiman, T. H. (1960). Stimulated optical radiation in ruby.

Mao, Q., Jiang, J., Li, X., Chang, J., & Liu, W. (2009). Widely tunable continuous wave mid-IR DFG source based on fiber lasers and amplifiers. *Laser Physics Letters, 6*(9), 647-652.

Markatos, S., Ayres, S., Kreit, D., Kerr, A., Youngquist, R., & Giles, I. (1987). *Optical fibre switch.* Paper presented at the Fiber Optic Sensors II.

May, P., Khan, U., Hughes, J. M., & Coleman, J. N. (2012). Role of solubility parameters in understanding the steric stabilization of exfoliated two-dimensional nanosheets by adsorbed polymers. *The Journal of Physical Chemistry C, 116*(20), 11393-11400.

Nishizawa, N. (2014). Ultrashort pulse fiber lasers and their applications. *Japanese Journal of Applied Physics, 53*(9), 090101.

Novoselov, K., Jiang, D., Schedin, F., Booth, T., Khotkevich, V., Morozov, S., & Geim, A. (2005). Two-dimensional atomic crystals. *Proceedings of the National Academy of Sciences, 102*(30), 10451-10453.

Park, K., Lee, J., Lee, Y. T., Choi, W. K., Lee, J. H., & Song, Y. W. (2015). Black phosphorus saturable absorber for ultrafast mode-locked pulse laser via evanescent field interaction. *Annalen der Physik, 527*(11-12), 770-776.

Polak, A., & Stothard, D. J. (2018). *Enhanced photoacoustic spectroscopy sensitivity through intra-cavity OPO excitation.* Paper presented at the Chemical, Biological, Radiological, Nuclear, and Explosives (CBRNE) Sensing XIX.

Popa, D., Sun, Z., Hasan, T., Torrisi, F., Wang, F., & Ferrari, A. (2011). Graphene Q-switched, tunable fiber laser. *Applied Physics Letters, 98*(7), 073106.

Popa, D., Sun, Z., Torrisi, F., Hasan, T., Wang, F., & Ferrari, A. (2010). Sub 200 fs pulse generation from a graphene mode-locked fiber laser. *Applied Physics Letters, 97*(20), 203106.

Rahman, M., Dhar, A., Das, S., Dutta, D., Paul, M. C., Rusdi, M., . . . Harun, S. (2018). An 8 cm long holmium-doped fiber saturable absorber for Q-switched fiber laser generation at 2-µm region. *Optical Fiber Technology, 43*, 67-71.

Ravi, O., Prasad, K., Jain, R., Venkataswamy, M., Chaurasia, S., & Deva Prasad Raju, B. (2017). Lasing transition at 1.06 µm emission in Nd3+-doped borate-based tellurium calcium zinc niobium oxide glasses for high-power solid-state lasers. *Luminescence, 32*(5), 688-694.

Ren, A., Feng, M., Song, F., Ren, Y., Yang, S., Yang, Z., . . . Tian, J. (2015). Actively Q-switched ytterbium-doped fiber laser by an all-optical Q-switcher based on graphene saturable absorber. *Optics Express, 23*(16), 21490-21496.

Richardson, D., Nilsson, J., & Clarkson, W. (2010). High power fiber lasers: current status and future perspectives. *JOSA B, 27*(11), B63-B92.

Roxlo, C., Chianelli, R., Deckman, H., Ruppert, A., & Wong, P. (1987). Bulk and surface optical absorption in molybdenum disulfide. *Journal of Vacuum Science & Technology A: Vacuum, Surfaces, and Films, 5*(4), 555-557.

Roxlo, C., Daage, M., Leta, D., Liang, K., Rice, S., Ruppert, A., & Chianelli, R. (1986). Catalytic defects at molybdenum disulfide "edge" planes. *Solid State Ionics, 22*(1), 97-104.

Russell, P. S. J. (2006). Photonic-crystal fibers. *Journal of lightwave technology, 24*(12), 4729-4749.

Schepler, K. L., Smith, B. D., Heine, F., & Huber, G. (1993). *Passive Q-switching and mode locking of 2-um lasers.* Paper presented at the Solid State Lasers IV.

Senosiain, J., Díaz, I., Gastón, A., & Sevilla, J. (2001). High sensitivity temperature sensor based on side-polished optical fiber. *IEEE Transactions on Instrumentation and Measurement, 50*(6), 1656-1660.

Shi, W., Fang, Q., Zhu, X., Norwood, R., & Peyghambarian, N. (2014). Fiber lasers and their applications. *Applied optics, 53*(28), 6554-6568.

Shivananju, B. N., Yu, W., Liu, Y., Zhang, Y., Lin, B., Li, S., & Bao, Q. (2017). The Roadmap of Graphene-Based Optical Biochemical Sensors. *Advanced Functional Materials, 27*(19), 1603918.

Slusher, R. (1999). Laser technology. *Reviews of Modern Physics, 71*(2), S471.

Soltanian, M., Sharbirin, A., Ariannejad, M., Amiri, I., De La Rue, R., Brambilla, G., . . . Ahmad, H. (2016). Variable Waist-Diameter Mach–Zehnder Tapered-Fiber Interferometer as Humidity and Temperature Sensor. *IEEE Sensors Journal, 16*(15), 5987-5992.

Song, W., He, C., Zhang, W., Gao, Y., Yang, Y., Wu, Y., . . . Dong, Y. (2014). Synthesis and nonlinear optical properties of reduced graphene oxide hybrid material covalently functionalized with zinc phthalocyanine. *Carbon, 77*, 1020-1030.

Song, Y.-W., Jang, S.-Y., Han, W.-S., & Bae, M.-K. (2010). Graphene mode-lockers for fiber lasers functioned with evanescent field interaction. *Applied Physics Letters, 96*(5), 051122.

Song, Y.-W., Yamashita, S., Goh, C. S., & Set, S. Y. (2007). Carbon nanotube mode lockers with enhanced nonlinearity via evanescent field interaction in D-shaped fibers. *Optics letters, 32*(2), 148-150.

Sotor, J., Sobon, G., Grodecki, K., & Abramski, K. (2014). Mode-locked erbium-doped fiber laser based on evanescent field interaction with Sb2Te3 topological insulator. *Applied Physics Letters, 104*(25), 251112.

Spühler, G., Paschotta, R., Fluck, R., Braun, B., Moser, M., Zhang, G., . . . Keller, U. (1999). Experimentally confirmed design guidelines for passively Q-switched microchip lasers using semiconductor saturable absorbers. *JOSA B, 16*(3), 376-388.

Sun, Z., Hasan, T., Torrisi, F., Popa, D., Privitera, G., Wang, F., . . . Ferrari, A. C. (2010). Graphene mode-locked ultrafast laser. *ACS nano, 4*(2), 803-810.

Sun, Z., Martinez, A., & Wang, F. (2016). Optical modulators with 2D layered materials. *Nature photonics, 10*(4), nphoton. 2016.2015.

Sun, Z., Popa, D., Hasan, T., Torrisi, F., Wang, F., Kelleher, E. J., . . . Ferrari, A. C. (2010). A stable, wideband tunable, near transform-limited, graphene-mode-locked, ultrafast laser. *Nano Research, 3*(9), 653-660.

Tang, P., Zhang, X., Zhao, C., Wang, Y., Zhang, H., Shen, D., . . . Fan, D. (2013). Topological Insulator: $\hbox {Bi} _ {2}\hbox {Te} _ {3} $ Saturable Absorber for the Passive Q-Switching Operation of an in-Band Pumped 1645-nm Er: YAG Ceramic Laser. *IEEE Photonics Journal, 5*(2), 1500707-1500707.

Thurow, B. S., Satija, A., & Lynch, K. (2009). Third-generation megahertz-rate pulse burst laser system. *Applied optics, 48*(11), 2086-2093.

Tien, C.-L., Chen, H.-W., Liu, W.-F., Jyu, S.-S., Lin, S.-W., & Lin, Y.-S. (2008). Hydrogen sensor based on side-polished fiber Bragg gratings coated with thin palladium film. *Thin Solid Films, 516*(16), 5360-5363.

Toth, C. K., & Petrie, G. (2018). Introduction to laser ranging, profiling, and scanning *Topographic laser ranging and scanning* (pp. 1-28): CRC Press.

Tseng, S.-M., & Chen, C.-L. (1992). Side-polished fibers. *Applied optics, 31*(18), 3438-3447.

Unger, S., Lindner, F., Aichele, C., & Schuster, K. (2018). Rare-Earth-Doped Laser Fiber Fabrication Using Vapor Deposition Technique. *Handbook of Optical Fibers*, 1-20.

Wagoner, G. A., McCallion, K. J., & Jameson, G. O. (1999). Fiber optic attenuators and attenuation systems: Google Patents.

Wang, K., Wang, J., Fan, J., Lotya, M., O'Neill, A., Fox, D., . . . Zhao, Q. (2013). Ultrafast saturable absorption of two-dimensional MoS2 nanosheets. *ACS nano, 7*(10), 9260-9267.

Wang, Q. H., Kalantar-Zadeh, K., Kis, A., Coleman, J. N., & Strano, M. S. (2012). Electronics and optoelectronics of two-dimensional transition metal dichalcogenides. *Nature nanotechnology, 7*(11), 699.

Wang, S., Yu, H., Zhang, H., Wang, A., Zhao, M., Chen, Y., . . . Wang, J. (2014). Broadband few-layer MoS2 saturable absorbers. *Advanced materials, 26*(21), 3538-3544.

Wei, C., Luo, H., Zhang, H., Li, C., Xie, J., Li, J., & Liu, Y. (2016). Passively Q-switched mid-infrared fluoride fiber laser around 3 µm using a tungsten disulfide (WS2) saturable absorber. *Laser Physics Letters, 13*(10), 105108.

Wong, W. S., Chen, C.-J., & Sun, Y. (2017). Introduction to lasers and optical amplifiers. *Handbook of Optoelectronics: Concepts, Devices, and Techniques (Volume One)*, 175.

Woodward, R., Kelleher, E., Howe, R., Hu, G., Torrisi, F., Hasan, T., . . . Taylor, J. (2014). Tunable Q-switched fiber laser based on saturable edge-state absorption in few-layer molybdenum disulfide (MoS 2). *Optics express, 22*(25), 31113-31122.

Woodward, R. I., & Kelleher, E. J. (2015). 2D saturable absorbers for fibre lasers. *Applied Sciences, 5*(4), 1440-1456.

Wu, K., Zhang, X., Wang, J., Li, X., & Chen, J. (2015). WS 2 as a saturable absorber for ultrafast photonic applications of mode-locked and Q-switched lasers. *Optics express, 23*(9), 11453-11461.

Xia, F., Wang, H., & Jia, Y. (2014). Rediscovering black phosphorus as an anisotropic layered material for optoelectronics and electronics. *Nature communications, 5*, 4458.

Xie, G., Ma, J., Lv, P., Gao, W., Yuan, P., Qian, L., . . . Tang, D. (2012). Graphene saturable absorber for Q-switching and mode locking at 2 µm wavelength. *Optical Materials Express, 2*(6), 878-883.

Yamashita, S. (2012). A tutorial on nonlinear photonic applications of carbon nanotube and graphene. *Journal of lightwave technology, 30*(4), 427-447.

Yeom, D. I., Park, H. S., & Kim, B. Y. (2004). Tunable narrow-bandwidth optical filter based on acoustically modulated fiber Bragg grating. *IEEE Photonics Technology Letters, 16*(5), 1313-1315.

Young, Y. E., & Setzler, S. D. (2007). System and method for a passively Q-switched, resonantly pumped, erbium-doped crystalline laser: Google Patents.

Yu, Z., Song, Y., Tian, J., Dou, Z., Guoyu, H., Li, K., . . . Zhang, X. (2014). High-repetition-rate Q-switched fiber laser with high quality topological insulator Bi 2 Se 3 film. *Optics express, 22*(10), 11508-11515.

Zervas, M. N., & Codemard, C. A. (2014). High power fiber lasers: a review. *IEEE Journal of selected topics in Quantum Electronics, 20*(5), 219-241.

Zhang, H. (2015). Ultrathin two-dimensional nanomaterials. *ACS nano, 9*(10), 9451-9469.

Zhang, L., Zhang, W., & Bennion, I. (2008). In-fiber grating optic sensors. *Fiber Optic Sensors*, 109-162.

Zhang, L., Zhuo, Z., Wang, J., & Wang, Y. (2012). Passively Q-switched fiber laser based on graphene saturable absorber. *Laser Physics, 22*(2), 433-436.

Zhang, Y., He, K., Chang, C.-Z., Song, C.-L., Wang, L.-L., Chen, X., . . . Shan, W.-Y. (2010). Crossover of the three-dimensional topological insulator Bi 2 Se 3 to the two-dimensional limit. *Nature Physics, 6*(8), 584.

Zhao, C., Zhang, H., Qi, X., Chen, Y., Wang, Z., Wen, S., & Tang, D. (2012). Ultra-short pulse generation by a topological insulator based saturable absorber. *Applied Physics Letters, 101*(21), 211106.

Zhao, J., Cao, S., Liao, C., Wang, Y., Wang, G., Xu, X., . . . Wang, Y. (2016). Surface plasmon resonance refractive sensor based on silver-coated side-polished fiber. *Sensors and Actuators B: Chemical, 230*, 206-211.

Zhao, J., Yin, G., Liao, C., Liu, S., He, J., Sun, B., . . . Wang, Y. (2015). Rough side-polished fiber with surface scratches for sensing applications. *IEEE Photonics Journal, 7*(3), 1-7.

Zhao, L., Tang, D., Zhang, H., Wu, X., Bao, Q., & Loh, K. P. (2010). Dissipative soliton operation of an ytterbium-doped fiber laser mode locked with atomic multilayer graphene. *Optics letters, 35*(21), 3622-3624.

Zheng, S., Ghandehari, M., & Ou, J. (2016). Photonic crystal fiber long-period grating absorption gas sensor based on a tunable erbium-doped fiber ring laser. *Sensors and Actuators B: Chemical, 223*, 324-332.

Zhu, W., Qian, L., & Helmy, A. S. (2007). Implementation of three functional devices using erbium-doped fibers: An advanced photonics lab. *Laser, 1520*, 1570nm.

LIST OF PUBLICATIONS AND PAPERS PRESENTED

1) Ahmad, H., Amiri, I. S., Zulkifli, A. Z., Hassan, H., Safaei, R., & Thambiratnam, K. (2017). Stable dual-wavelength erbium-doped fiber laser using novel fabricated side-polished arc-shaped fiber with deposited ZnO nanoparticles. *Chinese Optics Letters*, *15*(1), 011403.

2) Ahmad, H., Hassan, H., Safaei, R., Thambiratnam, K., Ismail, M. F., & Amiri, I. S. (2017). Molybdenum disulfide side-polished fiber saturable absorber Q-switched fiber laser. *Optics Communications*, *400*, 55-60.

3) Ahmad, H., Hassan, H., Safaei, R., Thambiratnam, K., & Amiri, I. S. (2017). Q-switched fiber laser using carbon platinum saturable absorber on side-polished fiber. *Chinese Optics Letters*, *15*(9), 090601.

4) Hassan, H., Ariannejad, M. M., Safaei, R., Amiri, I. S., & Ahmad, H. (2017, June). Mode-locked Erbium-doped fiber laser generation using hybrid ZnO/GO saturable absorber. In *IOP Conference Series: Materials Science and Engineering*(Vol. 210, No. 1, p. 012046). IOP Publishing.

5) Ahmad, H., Hassan, H., Zulkifli, A. Z., Thambiratnam, K., & Amiri, I. S. (2017). Characterization of arc-shaped side-polished fiber. *Optical and Quantum Electronics*, *49*(6), 207

APPENDICES